Surface and aerodynamic roughness in arid and semiarid areas andtheir relation to radar backscatter coefficient

Beatrice Marticorena, Mouldi Kardous, Gilles Bergametti, Yann Callot, Patrick Chazette, Houcine Khatteli, Sylvie Le Hégarat-Mascle, Michel Maille, Jean-Louis Rajot, Daniel Vidal-Madjar, et al.

Surface and aerodynamic roughness in arid and semiarid areas and their relation to radar backscatter coefficient

Béatrice Marticorena,[1] Mouldi Kardous,[2] Gilles Bergametti,[1] Yann Callot,[3,4] Patrick Chazette,[5] Houcine Khatteli,[2] Sylvie Le Hégarat-Mascle,[6] Michel Maillé,[1] Jean-Louis Rajot,[1,7] Daniel Vidal-Madjar,[6,8] and Mehrez Zribi[6]

Received 6 January 2006; revised 27 March 2006; accepted 25 April 2006; published 23 September 2006.

[1] Surface roughness is a key parameter for surface-atmosphere exchanges of mass and energy. Only a few field measurements have been performed in arid or semiarid areas where it is an important control of the aeolian erosion threshold. An intensive field campaign was performed in southern Tunisia to measure the lateral cover, L_c, and the aerodynamic roughness length, Z_0, over 10 sites with different surface roughnesses. L_c was determined by combining field measurements of the geometry of the roughness elements and simple assumptions on their shapes. Z_0 was experimentally determined from high-precision wind velocity and air temperature profiles. The resulting data were found to be in good agreement with the existing relationships linking the geometric and the aerodynamic roughness. This suggests that for natural surfaces, Z_0 can be estimated on the basis of the geometric characteristics of the roughness elements. This data set was then used to investigate the capabilities of radar backscatter coefficients, σ_0, to retrieve L_c and/or Z_0. Significant relationships were found between σ_0 and both L_c and Z_0. The SAR/ERS data set is in agreement with the SIR-C SLR data set from Greeley et al. (1997). On the basis of these two data sets including data from different arid and semiarid areas (North Africa, South Africa, North America), we propose an empirical relationship to retrieve Z_0 using radar observations in the C band from operational sensors.

Citation: Marticorena, B., et al. (2006), Surface and aerodynamic roughness in arid and semiarid areas and their relation to radar backscatter coefficient, *J. Geophys. Res.*, *111*, F03017, doi:10.1029/2006JF000462.

1. Introduction

[2] Surface roughness controls the transfer of momentum from the atmosphere to the Earth surface. Thus it is a key parameter to estimate mineral dust emissions resulting from wind erosion of arid and semiarid land surfaces. For a given wind velocity, the surface wind shear stress, τ, and thus the wind friction velocity increases with the surface roughness. However, an increase in surface roughness also leads to an increase of the erosion threshold wind friction velocity (also called erosion threshold) [*Marticorena et al.*, 1997a]. The roughness elements present on the surface absorb a part of the wind shear stress leading to an apparent increase of this erosion threshold. This latter effect is predominant, and a decrease of the soil losses due to wind erosion is generally observed when the surface roughness increases [*Wolfe and Nickling*, 1996].

[3] The assessment of the wind erosion intensity and of the mineral dust emissions requires a precise estimation of the erosion thresholds as a function of the local surface roughness. In arid areas, the surface roughness is mainly controlled by inert nonerodible elements having centimetric to metric sizes, such as boulders, pebbles, gravel, sand grains, etc., and by vegetation. In semiarid areas, vegetation cover is a major component of the surface roughness.

[4] Recently, physical models have been developed to account for the influence of the surface characteristics on the dust emission, including explicit parameterizations of the aeolian erosion threshold as a function of the surface roughness [*Marticorena and Bergametti*, 1995; *Shao et al.*, 1996]. *Marticorena and Bergametti* [1995] have developed a drag partition scheme to describe the increase of the threshold wind friction velocity as a function of the aerodynamic roughness length, Z_0, which can be experimentally derived from vertical profiles of dynamical parameters: wind velocity, air temperature and humidity. *Shao et al.* [1996] and *Shao* [2001] have used an erosion threshold

[1] Laboratoire Interuniversitaire des Systèmes Atmosphériques, Universités Paris VII-XII, UMR CNRS 7583, Créteil, France.
[2] Institut des Régions Arides, Médénine, Tunisia.
[3] Faculté Géographie, Histoire, Histoire de l'Art, Tourisme, et Laboratoire Institut de Recherche en Géographie, Université Lyon 2, Bron, France.
[4] Also at Archéorient, UMR CNRS 5133, Maison de l'Orient Méditerranéen, Lyon, France.
[5] Laboratoire des Sciences du Climat et de l'Environnement, Commissariat à l'Energie Atomique, UMR CNRS 1572, Saclay, France.
[6] Centre d'étude des Environnements Terrestres et Planétaires, UMR CNRS 8639, Vélizy, France.
[7] Also at Institut pour la Recherche et le Développement, Niamey, Niger.
[8] Also at Direction des Ressources Humaines, CNRS, Paris, France.

0148-0227/06/2006JF000462

parameterization derived from theoretical considerations on the drag partition [*Raupach*, 1992]. This parameterization is based on the roughness density, or lateral cover, L_c, and on the ratio between the drag coefficients for isolated roughness elements and the drag coefficient of a bare surface [*Raupach et al.*, 1993]. The lateral cover represents the total silhouette area of the roughness elements per unit of horizontal surface. It characterizes the surface geometric roughness. One way to summarize the relationship between the drag and geometric properties is to plot the ratio of aerodynamic roughness length to the mean height of the obstacles, Z_0/h versus the lateral cover L_c [*Raupach*, 1992]. On the basis of wind-tunnel measurements for rough surfaces made of artificial compact roughness elements, an empirical relationship was established between Z_0/h and L_c [*Marticorena et al.*, 1997b].

[5] However, the surface roughness of natural arid and semiarid areas is poorly documented in the literature. In particular, very few field measurements of both aerodynamic roughness and geometrical characteristics of the surface are available for these regions [*Lancaster*, 2004; *Lancaster and Baas*, 1998]. As a result, practical application of the empirical relationships previously established between aerodynamic and geometric roughness to natural desert surfaces, and especially to sparsely vegetated surfaces, remains questionable [*Gillies et al.*, 2000; *King et al.*, 2005]. Moreover, the few existing experimental data sets are largely insufficient to allow the mapping of surface roughness as required for the estimation of mineral dust emissions at a global scale.

[6] *Callot et al.* [2000] have proposed a method to estimate the aerodynamic roughness length based on a geomorphologic approach. They applied this method to map the surface roughness over the Sahara and the Arabian Peninsula with a spatial resolution of $1° \times 1°$. The mineral dust emissions simulated at the continental scale with this data set were found in agreement with the dust indexes derived from satellite observations [*Marticorena et al.*, 1997b]. However, the application of such an approach to other arid areas is difficult since it requires (1) exhaustive and accurate documentation of these arid areas and (2) field observations to precisely calibrate the mapped information. As a result, the confidence level of the results derived from this geomorphologic approach may significantly vary from one arid area to the other.

[7] *Greeley et al.* [1991] have tested the capability of radar measurements to retrieve the surface roughness in arid areas. These authors propose an empirical relationship linking in situ measurements of aerodynamic roughness lengths and radar backscatter cross sections σ_0 derived from airborne (NASA airborne radar system, AIRSAR) and spaceborne (Shuttle Radar Laboratory onboard the Shuttle Endeavour, April and October 1994) observations [*Greeley et al.*, 1997]. However, this study was not extended to routinely available spaceborne observations, which are the only ones having the potential for mapping the aerodynamic roughness lengths over the whole desert areas.

[8] In this paper, we present results obtained during an intensive field experiment performed in South Tunisia during spring 2000 and dedicated to measurements of the geometric and aerodynamic surface roughness. The results allow us to test the relationships linking these two types of roughness for natural surfaces. They also offer the opportunity to test the capability of an operational spaceborne radar system to retrieve the surface roughness over arid and semiarid surfaces. The relationships between the geometric roughness, the aerodynamic roughness length and the radar backscatter coefficient derived from the measurements of the Synthetic Aperture Radar (SAR) onboard the Earth Resource Satellite (ERS) from the European Space Agency (ESA) are investigated. Such a relationship should allow the mapping of the aerodynamic roughness lengths over any arid surface with a spatial resolution of 30 m.

2. Experimentation

2.1. Description of the Experimental Sites

2.1.1. General Characteristics of the Studied Area

[9] The experiment took place in March 2000 for several sites located in the south of Tunisia with different surface roughness characteristics.

2.1.1.1. Climatic Conditions

[10] Southern Tunisia experiences an arid climate. Annual precipitations are small, generally less than 200 mm. The evapotranspiration is very intense owing to the high temperatures and is accentuated by the drying capacity of the wind. Moreover, precipitation is irregular in space and time, most of the rainfall falling from autumn to spring. The precipitation rates measured between 1993 and 2003 in several meteorological stations of South Tunisia (Djerba, Kébili, Médénine, Remada, and Tozeur) reveal a significant deficit ($\sim$50%) in the period 1998–2001 compared to the 10 years averaged (1993–2003) annual precipitations. The intensive experiment has thus taken place in very dry conditions.

2.1.1.2. Landscapes

[11] In the area where the experiment took place (Figure 1), the main landscape units are as follows.

[12] 1. The ''Matmatas mounts'' extend from north to south and separate the plain of Jeffara in the east from the Great Eastern Erg in the west. It is composed of a series of cuestas with altitudes ranging from 80 to 450 m and a maximum around 700 m. The surface is mainly rocky.

[13] 2. The ''plain of Jeffara'' is located in the northeastern part of the experimental region between Gabès and the Libyan border. The surface corresponds to a glacis pediment covered by different Quaternary accumulations with an important disturbance of the soil surface due to intense agricultural activities.

[14] 3. To the west, the Matmatas mounts lead to a high, flat and noncultivated plateau named ''Dahars.'' This large plateau (around 7800 km^2) extends toward the Great Eastern Erg. The surface is covered with stones and/or pebbles and the vegetation is mainly composed of small permanent bushes.

[15] 4. In the northwest of the experimental region, a closed ephemeral salty lake, called ''Chott El-Jerid,'' is located in a large depressed basin (10,500 km^2, [*Gueddari*, 1984]). This Chott is one of the evaporitic basins extending along the southern piedmont of the eastern extension of Saharan Atlas Mountain, in the ''low Sahara,'' from Biskra (Algeria) to the gulf of Gabès (Tunisia). With a surface of 5360 km^2 [*Millington et al.*, 1989], it is the largest salty dry lake in the north of Africa. This depression is supplied with

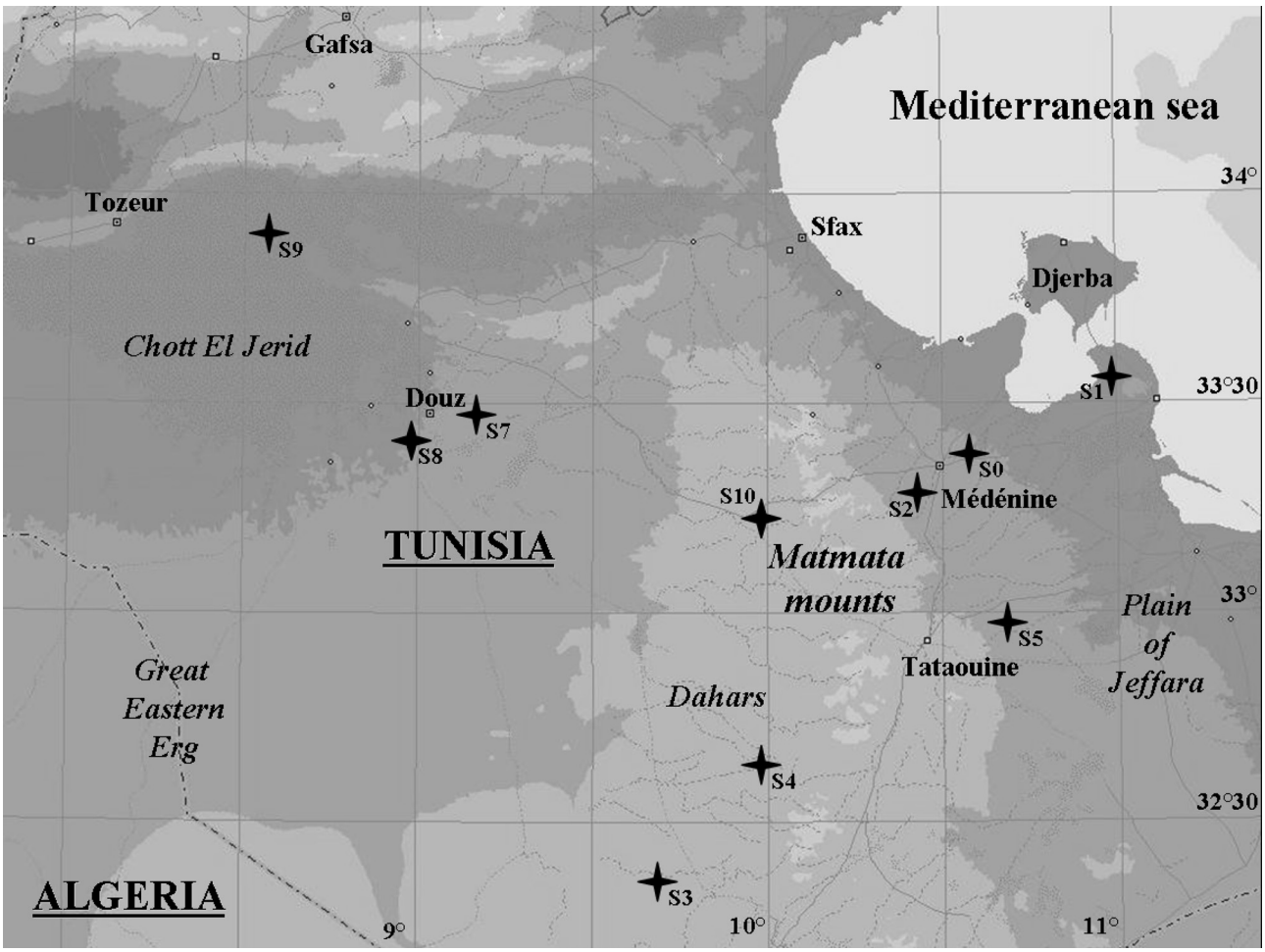

Figure 1. Map of South Tunisia and location of the experimental sites; shading corresponds to topography (dark gray, below sea level up to 50 m; light gray, 500–1000 m).

water by both rainfall and underground water, exhibiting occasionally surfaces of stagnant water. Crusted salty and silty sediments cover the largest fraction of the surface [*Rabia and Zargouni*, 1990] and a variety of salty crusts can be observed, ranging from thin silty crusts to salty fragmented pavements about 10 cm thick. Gypseous or calcareous crusts can also be found on its borders [*Rabia and Zargouni*, 1990].

2.1.1.3. Land Uses

[16] In this region, land use is connected to the agriculture. Along the coast, arboriculture and especially olive trees, constitute the main agricultural activity. Olive trees are extensively cultivated over a surface covering around 2500 km^2 that tends to extend more and more. The fields are composed of regularly spaced olive trees, and the soil surface is frequently ploughed between these trees to avoid water competition with natural vegetation and to save water by burying the moist soil fraction.

[17] Inland, up to the Matmatas, culture of cereals (wheat and barley) and market gardening are common practices. However, these activities depend strongly on the annual precipitation and on the availability of water for irrigation. They mainly concern small parcels, producing a quite patchy landscape. In the south of the Jeffara plain and in the Dahars plain, pasture activity is the dominant land use. In this area, many herds of goats, sheep or camels are grazing especially during spring and winter.

[18] Finally, the combination of these landscapes and land uses produces different surface features among which the most frequently encountered is a surface covered with stones and/or pebbles and vegetation characterized by small permanent bushes. The dimensions and cover rates of these two kinds of roughness elements depend on the geographical location and on the local precipitation rates. The size and covering rate of the permanent vegetation decrease along the distance from the coast to inland and from north to south, following the precipitation gradient. The size and rate of gravels, cobbles and boulders are mainly connected to the soil properties and to the distance of their main source (i.e., the mountain range of Matmata) even if stony surfaces can also be found in some other places, as for example close to Médénine. On the opposite, close to Douz, the calcareous substrate is covered with sand mixed with gypseous debris, with frequent limestone armour outcrops. The region presents also smoother surfaces such as the interdunal flat surface in the border of the Great Eastern Erg and the crusted surface of the Chott El Jerid.

2.1.2. Description of the Selected Sites

[19] Nine sites have been chosen in order to investigate a large range of surface roughness. These sites were also

Table 1. Locations, Geographical Coordinates, and Characteristics of the Experimental Sites

Site Number and Name	Geographical Coordinates	Landscape Type
S0, Dar Daoui	33°17′41″N–10°46′57″E	highly vegetated pasture range
S1, Chammakh	33°35′40″N–10°59′34″E	olive tree plantation
S2, South of Médénine	33°15′40″N–10°28′13″E	degraded stony pasture range
S3, South of Ksar Ghilane	32°42′47″N–09°41′44″E	low vegetated, stony pasture range
S4, Bir Amir	32°37′07″N–09°58′43″E	sandy vegetated pasture range
S5, Maouna	33°01′21″N–10°40′20″E	vegetated, stony pasture range
S7, Douz-Matmata	33°27′12″N–09°14′36″E	slightly degraded gypseous pasture range
S8, Douz	33°25′38″N–09°02′08″E	sand dunes
S9, Chott El JErid	33°53′23″N–08°33′17″E	salty depression
S10, Bir Zoui	33°14′54″N–09°58′06″E	highly degraded pastureland

selected because they provide the fetch required for relevant wind profile measurements [*Wieringa*, 1993]. Four of the selected sites are located in the Jeffara plain (i.e., in cultivated or pasture areas) and three in the Dahars (i.e., in pasture areas). These different sites allowed sampling different vegetation and/or stone covers. Two additional sites were also investigated in order to document non-vegetated surfaces typical of arid regions, i.e., a dune field and a salty depression. The geographic coordinates and characteristics of the selected sites are given in Table 1. The species encountered on sites having a natural vegetation cover are listed in Table 2. Representative examples of the investigated sites and of their roughness characteristics are given in Figure 2.

[20] Site 1 is a typical olive tree plantation, in which olive trees are arranged in a square pattern. The olive trees, about 3 m height, are spaced 23 m. Sites 2 and 10, located respectively in the Jeffara plain and in the Dahars are highly degraded pasture ranges, the in-place vegetation being visibly reduced by grazing. Site 2 exhibits a higher stone cover than site 10. Site 3 is the most southern site and is characterized by a naturally low vegetation cover and a high stone cover. Site 7 is located in a sandy gypseous area in the northern part of the Dahars. It exhibits a low vegetation cover and a negligible stone cover. Sites 4 and 5 are both pasture range with a moderate vegetation cover, site 5 having a significant stone cover. All these sites (S2, S3, S4, S5, S7 and S10) exhibit a natural vegetation cover but this vegetation is composed of different species depending on the sites. Among the 12 identified species (Table 2), two species only (*Hammada schmittiana*, *Atractylis serratuloïdes*) are observed over three sites, and two others (*Gymnocorpos decander*, *Anthyllis Sericea*) are present on two sites.

[21] Site 8 is a flat interdunal area covered with very small gravels, located in a small sand sea with undulating dunes. Site 9 is located close to the center of the Chott El Jerid, where the surface is highly crusted but very flat. Site 6, quite similar to site 7, has finally been rejected owing to an undulating topography.

[22] Finally, the experimental setup has been first tested over a vegetated parcel in the experimental station of Institut des Régions Arides (IRA) (Dar Daoui, site 0), an area protected from agricultural and grazing activities for few years and thus for which the vegetation cover is important.

2.2. Methodology

[23] To investigate the relationship between the geometric and the aerodynamic roughness, both have been experimentally documented during a one month field campaign (March 2000). The duration of the experiment over each site was mainly controlled by the fulfilling of the conditions required for the aerodynamic measurements (see below). Once satisfying dynamical measurements were obtained, the experimental setup was moved to the next site. Generally, the experimental period was of about 3 days per site. Measurements of the geometric characteristics of the roughness elements were performed during the period corresponding to the aerodynamic measurements.

2.2.1. Lateral Cover L_c

[24] Among the different parameters characterizing the surface roughness, the lateral cover L_c, also called roughness density, is commonly used as a measure of the roughness characteristic [see, e.g., *Musick and Gillette*, 1990]. The interaction between the wind shear stress and the surface roughness is directly dependent on the vertical surface of obstacles exposed to the wind. The lateral cover is thus defined as the sum of the frontal silhouette areas of the obstacles present on the surface and facing the wind direction divided by the surface,

$$L_c = \frac{ns}{S} = \frac{\sum_{i=1}^{i=n} s_i}{S}, \tag{1}$$

where n and s are, respectively, the number and the mean frontal silhouette area of the obstacles present over a given horizontal surface area, S. The mean frontal silhouette area (s) can be computed from the geometrical dimensions of the obstacles, given the shape of the obstacles. On the basis of this definition, the lateral cover L_c can be estimated by counting the obstacles present on a representative surface and by measuring their geometrical dimensions.

Table 2. Vegetation Species Identified Over the Vegetated Experimental Sites

Vegetation Species (Latin Name)	Site Number					
	S2	S3	S4	S5	S7	S10
Gymnocorpos decander	yes	no	no	no	no	yes
Astragalus armatus	yes	no	no	no	no	no
Rhantérium suaveolens	yes	no	no	no	no	no
Hammada schmittiana	no	yes	no	yes	yes	no
Anthyllis Sericea	no	yes	yes	no	no	no
Atractylis serratuloïdes	no	no	yes	yes	no	yes
Hammada scoparia	no	no	no	yes	no	no
Retama raetam	no	no	no	no	yes	no
Zygophyllum album	no	no	no	no	yes	no
Anarrhinum brevifolium	no	no	no	no	yes	no
Oudneya africana	no	no	no	no	yes	no
Helianthemum kahiricum	no	no	no	no	no	yes

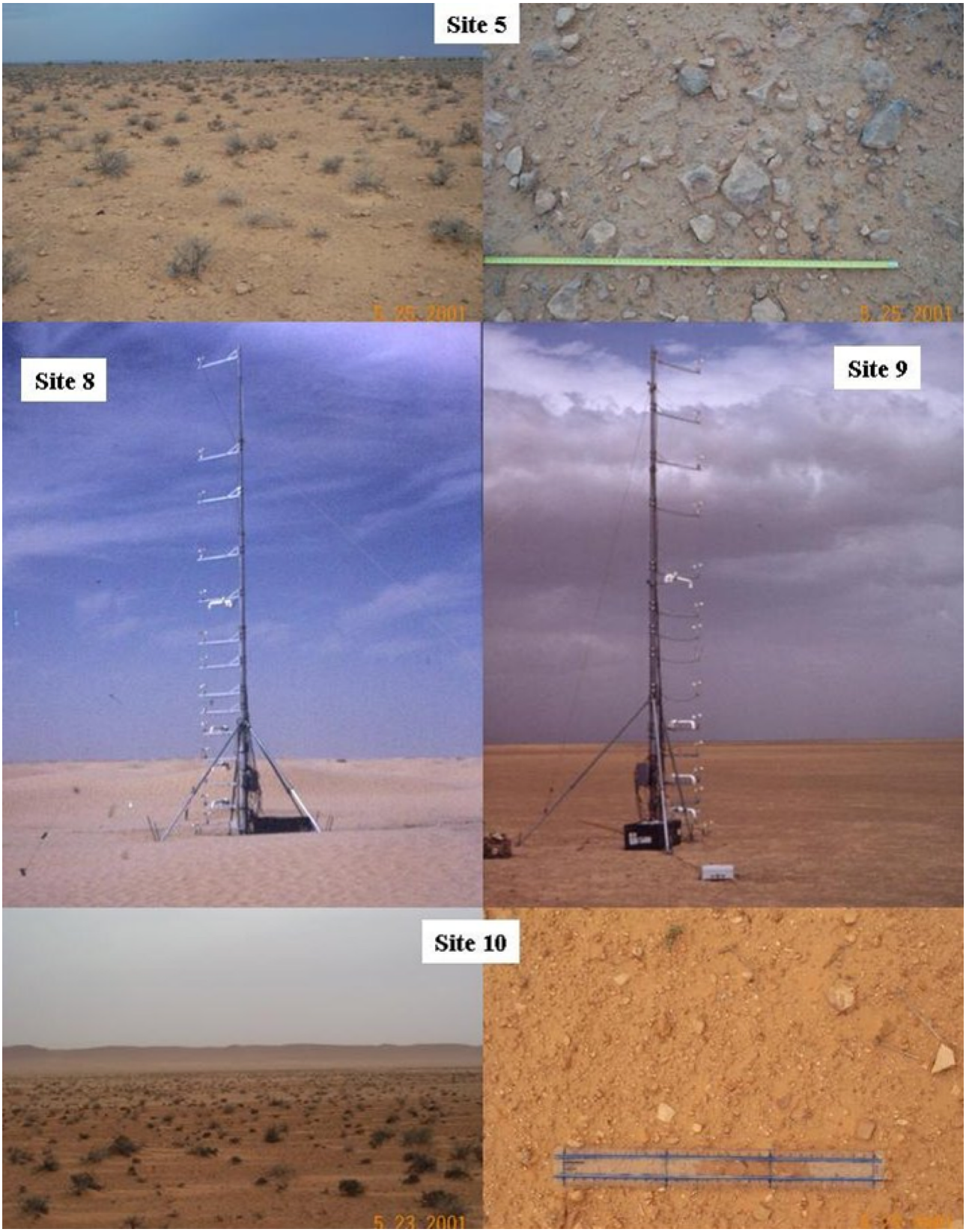

Figure 2. Photographs of representative examples of the sites investigated, showing the experimental setup and the range of roughness sampled (vegetation + pebbles): site 5 (Maouna), a rough site; site 10 (Bir Zoui) a moderately rough site; and sites 8 (Douz dune field) site 9 (Chott Jerid), smooth sites.

Table 3. Number, Mean, and Mean Deviation of Height and Width of the Vegetation Elements and Pebbles for the Different Experimental Sites[a]

	Vegetation			Pebbles and Gravel		
Site Number	Number (for 100 m)	Height, cm (Median, std)	Width, cm (Median, std)	Number (for 20 m)	Height, cm (Median, std)	Width, cm (Median, std)
S2	91	15.0 (9.1)	20 (16)	19	1.4 (0.8)	2.5 (0.7)
S3	65	10.0 (5.0)	17 (9.0)	94	0.75 (0.5)	2.75 (1.1)
S4	108	15.0 (9.3)	24.5 (16)	99	1.0 (0.6)	3.0 (1.0)
S5	63	15.0 (9.9)	30 (20)	163	2.0 (1.2)	4.0 (2.6)
S7	19	14.0 (7.8)	25 (15)	3	1.5 (0.9)	2.0 (0.9)
S10	49	5.0 (8.1)	15 (4.7)	53	1.5 (0.9)	3.0 (0.7)

[a]Except sites S0, S1, S8, and S9, for which geometrical roughness measurements have not been performed.

2.2.1.1. Measurements of the Geometric Dimensions of Obstacles

[25] The vegetation cover being very low in such semi-arid areas, the sampled surface must be relatively large in order to include a statistically representative number of vegetation elements. However, owing to their relative large number, the measurements of the small pebbles can hardly be performed over a large surface. We thus decided to adopt a line-intercept method rather than the more often used surface area counting method, or quadrat method [e.g., *Wolfe and Nickling*, 1996] in order to cover as large an area as possible in the short time available [*Lancaster*, 2004]. We first measured the height and width of every rock larger than 0.01 m in diameter and every vegetation element intersected by the tape of a 20-m- long transect randomly located. Measurements for vegetation were repeated along four additional transect, i.e., a total sampled length of 100 m. The measured dimensions are the maximum height and width of the roughness elements in the direction of the transect.

[26] The results of these measurements for the sites exhibiting identifiable surface roughness elements (i.e., for all sites except the sand dunes and the salty depression) are reported in Table 3. The number of pebbles varies significantly from one site to the other, with extreme values of 3 for site 7 and 163 for site 5. In contrast, the geometrical characteristics of the pebbles do not differ very much from one site to the other: their median height ranges between 0.75 and 1.5 cm and their median width from 2 to 4 cm, except for site 5 where they are slightly higher and larger. The distributions of the height and width for all the sampled sites appear close to lognormal (Figure 3) with a median ratio of width to height of 2.5 and a standard deviation of 2.1.

[27] All the characteristics of the vegetation, i.e., height, width and number, vary significantly for the different sites. However, at each site there is a significant correlation between the height and the width of the individual bushes (Figure 4). For the whole data set (n = 375), the correlation coefficient, r, equals 0.77, but it ranges from 0.47 (site 7; n = 19) to 0.88 (site 4; n = 108) for the different sites. The slope of the linear relationship is 0.54 for the whole data set. It is close to 0.60 for sites 2, 3 and 4 for which r ranges from 0.75 to 0.89 and slightly lower, from 0.43 to 0.49 for the other sites (S5, S7 and S10). It must be noted that only two different species have been observed over sites 3 and 4, while 5 different species have been identified over site 7 (Table 2).

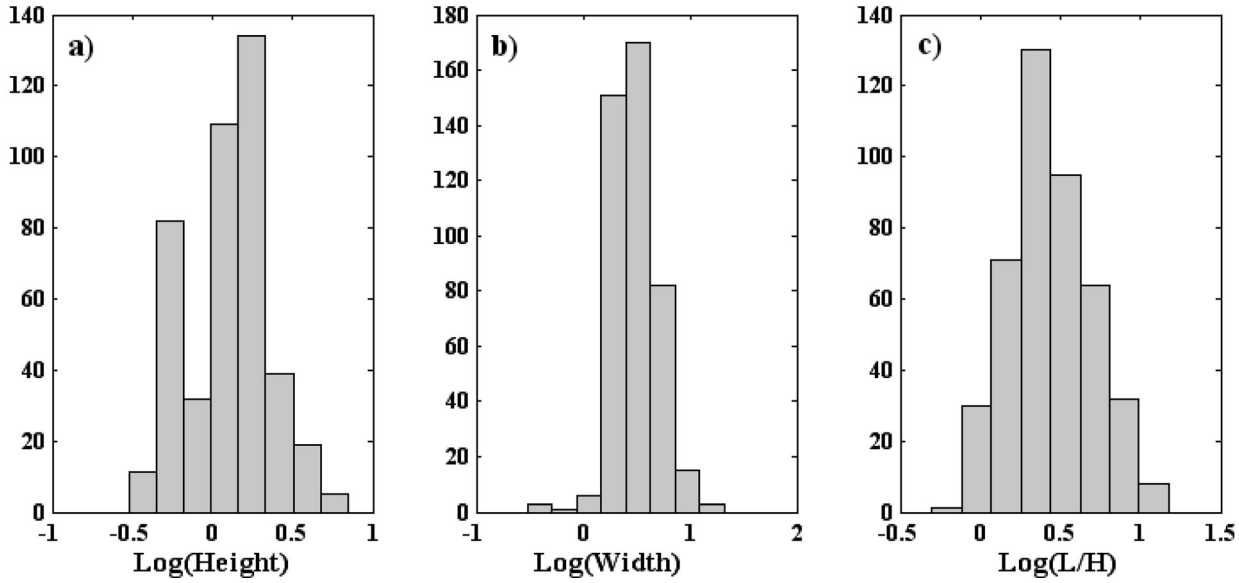

Figure 3. Number distribution of the logarithm of (a) the height (cm), (b) the width (cm), and (c) the ratio of width to height of the pebbles for all the sampled sites.

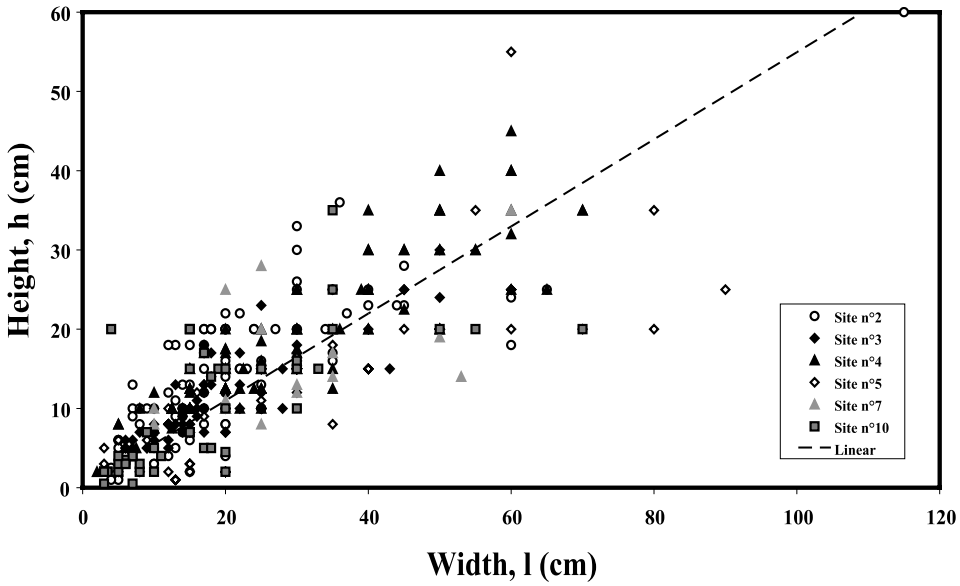

Figure 4. Vegetation height as a function of vegetation width. The dashed line represents the best linear fit (y = 0.54 x; r = 0.77; n = 375).

The degree of diversity of the vegetation species may partly explain the differences in the level of correlation between the geometrical dimensions of vegetation. Anyway, this general trend suggests that the individual bushes are, on average, roughly twice as wide as they are tall.

2.2.1.2. Determination of the Lateral Cover

[28] Assumptions on the roughness element shapes allow a determination of the lateral cover from the geometrical dimensions of the roughness element. From direct observations and photographs of the different types of obstacles, we adopted a half ellipsoid shape for vegetation and a rectangular shape for the boulders and pebbles.

[29] The area of an ellipse is given by: $\pi\, ab/4$, a being the short axis and b the long axis of the ellipse. This equation can be applied to the vegetation elements with $h = a/2$ and $l = 2b$. The frontal surface of the vegetation elements is thus given by

$$s_i = \frac{1}{2}\pi\, h_i \frac{l_i}{2}, \tag{2}$$

with h_i and l_i being, respectively, the height and width of the vegetation elements.

[30] For the pebbles and boulders, it is given by

$$s_i = h_i l_i, \tag{3}$$

with h_i and l_i being the height and width of the pebbles.

[31] The computation of L_c also needs to scale the one dimensional measurements performed along the transect to two dimensional parameters. This scaling is based on the assumption that the lateral surface of each obstacle refers to a horizontal surface given by

$$S_i = l_i \times L_t, \tag{4}$$

with L_t being the length of the transect.

[32] Then, for vegetation, L_c is computed as follows:

$$L_c = \sum_{i=1}^{i=n} \frac{\frac{1}{2}\pi\, h_i \frac{l_i}{2}}{l_i L_t} = \frac{1}{4}\frac{\pi}{L_t}\sum_{i=1}^{i=n} h_i, \tag{5}$$

and for boulders or pebbles,

$$\lambda = \sum_{i=1}^{i=n} \frac{h_i l_i}{l_i L_t} = \frac{1}{L_t}\sum_{i=1}^{i=n} h_i. \tag{6}$$

Applying these relations to the field measurements allowed an estimation of percent cover and lateral cover, respectively, due to vegetation and to boulders, the total covering rate and the total lateral cover being the sum of these two components.

[33] For the different sites, the total lateral cover ranges over almost 1 order of magnitude (from 0.025 to 0.233) (Table 4) with sites 4 and 5 having the highest total L_c and sites 10 and 7 the lowest. The lateral cover due to pebbles varies from 70% (site 5) to 8% (site 7), these values being associated respectively to the highest and the lowest total L_c. For sites 2, 7 and 4, vegetation is the dominant contributor to the total L_c, while for sites 3, 5 and 10, the lateral cover due to vegetation and to pebbles are comparable (Figure 5).

2.2.1.3. Uncertainties

[34] Uncertainties associated to these values mainly result from both the experimental approach, i.e., the so-called transect method, and from the assumptions made on the shape of the roughness elements. Uncertainties induced by the assumptions made on the shape of the obstacles are difficult to assess, since the shape of the individual roughness elements can hardly be determined. In this work, we assumed a rectangular shape for the pebbles and cobbles, and a half ellipsoid shape for the bushes. From counting and measurements performed in Tunisia, *Escadafal* [1989] assumed ellipsoid shape with a two-thirds flatness for pebbles

Table 4. Lateral Cover and Cover Percent Due to Vegetation and Pebbles, and Total Lateral Cover and Cover Percent Obtained for Sites 2, 3, 4, 5, 7, and 10

	Vegetation		Pebbles and Gravel		Total	
Site Number	Cover, %	Lateral Cover	Cover, %	Lateral Cover	Cover, %	Lateral Cover
2	15.6	0.106	2.17	0.013	17.8	0.119
3	9.3	0.056	11.3	0.041	20.6	0.097
4	24.0	0.152	12.4	0.058	36.4	0.21
5	15.8	0.071	29.9	0.162	45.7	0.233
7	4.34	0.023	0.30	0.002	4.64	0.025
10	6.6	0.037	6.16	0.031	12.76	0.068

and half-hemispheric shape for bushes. From our data, assuming an ellipsoid shape instead of a rectangular for the pebbles and cobbles changes their frontal surface by about 5%. For vegetation elements, as previously mentioned, they are roughly twice larger than high. This indicates that the more frequent shape for the bushes is a half hemisphere. However, the dispersion of the data reveals some departure from model, due to flat or high bushes that can be accounted for with the half-ellipsoid shape assumption. As a result, the uncertainties due to the assumption on the roughness elements shape appear low.

[35] We first estimated the uncertainty induced by the fact that we measured the maximum dimension of the roughness elements (width and height) in the direction of the transect. Indeed, such a two-dimensional (2-D) approach would have required the determination of the dimension strictly aligned along the transect. Over several transects, we thus also measured the dimensions intercepting the transect. We compared the derived L_c to those obtained when using the maximum dimensions. The differences between the total L_c derived from these two approaches are 17% in average.

[36] To test the validity of this 2-D method for the vegetation, we compared it with a strict 3-D approach. For site 7, the vegetation elements have been totally counted and measured over a surface of 19 m $\times$ 19 m for one of the experimental sites. The dimensions of the bushes that have been measured are the maximum width and the width in the direction perpendicular to the maximum length and the maximum height. Two extreme values of L_c can then be estimated for this site: $0.015 < L_c < 0.021$. The average L_c estimated for the five sampled transects is 0.023 ± 0.010, i.e., close to the highest estimation deduced from the surface counting. This result suggests that the transect method probably tends to slightly overestimate L_c, at least for vegetation. Assuming the best estimated L_c as the mean of the two extreme values obtained for the 19 m $\times$ 19 m surface (i.e., 0.018), the transect method could overestimate L_c by about 27%. It must be noted that the total number of vegetation elements sampled by the five 20-m transects is only 19, while 183 bushes have been counted over the 19 m $\times$ 19 m surface. This low number of vegetation elements measured on the transects, which is due to the scarcity of the vegetation over site 7, may explain in a large part the difference observed between the two methods. This bias should be reduced for the other experimental sites where vegetation is always more important.

[37] In conclusion, these comparisons suggest that the uncertainty induced by the experimental 2-D procedure we used can be reasonably estimated of the order of 30%. This uncertainty is mainly related to the representativity of the sampled area and of the sampling method. In particular, for surfaces with low vegetation cover, it seems that the area counting method would be superior. For surfaces covered with boulders, pebbles and gravel, the transect method appears as a relevant approach to determine the Lateral cover with a good confidence level. For these two methods, however, the sampled surface/length must be defined in order to obtain a representative number of roughness elements.

2.2.2. Measurements of the Aerodynamic Roughness Length

[38] For each of the selected sites, the aerodynamic roughness lengths have been determined based on wind velocity and air temperature profiles.

2.2.2.1. Retrieval of the Aerodynamic Roughness Length

[39] Classically, the aerodynamic roughness length, Z_0, is experimentally derived from vertical profiles of the wind velocity. Theoretically, in neutral conditions (i.e., no vertical gradient of air temperature) and for a given homogeneous surface, a simple similarity hypothesis allows the description of the vertical distribution of the wind velocity: The vertical gradient of wind velocity $^{\delta U}/_{\delta Z}$ is assumed to be dependent only on the height Z, above the surface, as described by a log law [*Panofsky and Dutton*, 1984],
for $Z \gg Z_0$

$$U(Z) = \frac{U_*}{k} \ln\left(\frac{Z}{Z_0}\right), \tag{7}$$

where U_* is the wind friction velocity and k the Von Karman's constant ($k = 0.4$).

[40] The aerodynamic roughness length, Z_0, is introduced as a dimensional constant for the integration of the equation of the vertical profile. Numerically, it corresponds to the height above the surface at which the wind velocity reaches zero. However, this numerical definition has no actual physical meaning, since the logarithmic profile is valid only above the roughness height. Typically, the log law is considered as valid for levels higher than twice the mean height of the obstacles inducing the surface roughness. In order to compare data from vegetated and bare surfaces, we

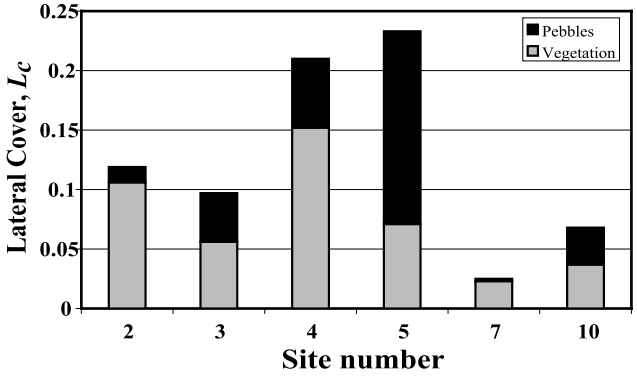

Figure 5. Contribution of vegetation and of the pebbles and gravel to the total lateral cover for sites 2, 3, 4, 5, 7, and 10.

did not use a wind profile equation including a displacement height. The excellent fit of the wind profile data to equation (7) suggests, however, that the actual displacement height was negligible.

[41] In natural conditions, neutrality only occurs at specific periods, generally close to the sunrise and before the sunset. During the rest of the day, turbulent exchanges between the surface and the atmosphere produce a thermal stratification of the surface layer. The similarity theory of *Monin and Obukhov* [1954] allows a reasonable description of the experimental micrometeorological data [see, e.g., *Arya*, 1988]. This theory describes the vertical profiles of wind velocity $U(Z)$ for turbulent fluxes in the surface boundary layer by the following equation:

$$U_{(Z)} = \frac{U*}{k} \cdot \left[\ln\left(\frac{Z}{Z_0}\right) - \Psi_m\left(\frac{Z}{L}\right) + \Psi_m\left(\frac{Z_0}{L}\right)\right], \quad (8)$$

with $L = \frac{U_*^2 \theta}{kg\theta_*}$, the Monin-Obukhov length (having length unit), and Ψ_m and Ψ_h the stability functions, m and h referring respectively to the momentum and the heat, θ the potential temperature and θ_* the temperature scale.

[42] A similar equation can be written for the vertical profile of air temperature, including a "thermal" roughness length, whose accurate determination would require a precise experimental determination of the surface temperature. Owing to the high heterogeneity of the surface which is composed of bare soil, pebbles and vegetation, relevant measurements of the soil temperature are difficult to perform. Thus we favored a description of the temperature gradient between two levels, Z_1 and Z_2, to avoid using the thermal roughness length,

$$\Delta\theta = \theta(Z_2) - \theta(Z_1) = \frac{\theta*}{k} \cdot \left[\ln\left(\frac{Z_1}{Z_2}\right) - \Psi_h\left(\frac{Z_2}{L}\right) + \Psi h\left(\frac{Z_1}{L}\right)\right]. \quad (9)$$

[43] The expressions of the stability functions Ψ_m and Ψ_h depend on the stability conditions in the surface layer, described by the stability parameter Z/L. This parameter represents the relative weight of buoyancy compared to the friction in the stratified surface layer.

[44] For $Z/L < 0$ (unstable conditions)

$$\Psi_m = \ln\left(\frac{1+x}{2}\right) + \ln\left(\frac{1+x^2}{2}\right) - 2\arctan(x) + \frac{\pi}{2} \quad (10)$$

$$\Psi_h = \ln\left(\frac{1+y}{2}\right), \quad (11)$$

with $x = [1-15\ Z/L]^{1/4}$ and $y = [1-15\ Z/L]^{1/2}$;

[45] For $Z/L > 0$ (stable conditions)

$$\Psi_m = \Psi_h = -5\ Z/L. \quad (12)$$

From its definition, it appears clearly that L varies from $+\infty$ to $-\infty$, the extreme values corresponding to situations for which the heat flux tends to zero (neutrality) either from the positive part (stable) or the negative part (unstable). The stability conditions can also be defined as a function of the Richardson number, R_i, as expressed by the following equations used to retrieve R_i from L [*Arya*, 1988],

[46] For $R_i > 0$

$$Z_m/L = R_i(Z_m) \quad (13)$$

[47] For $0 \leq R_i < 0.2$

$$Z_m/L = \frac{R_i(Z_m)}{[1 - 5\ R_i(Z_m)]}, \quad (14)$$

with $Z_m = (Z_{min} \cdot Z_{max})^{1/2}$.

[48] An iterative fitting procedure of the average of the measured wind velocities and air temperature with these equations allows the determination of the dynamical parameters $U*$, $\theta*$ and Z_0 in either stable or instable conditions (gradient method). Such a procedure was optimized by *Frangi and Richard* [2000].

2.2.2.2. Experimental Setup

[49] The experimental setup (Figure 1) was designed following the recommendations from *Wieringa* [1993]. The wind velocity and air temperature profiles were measured using a 10-m telescopic mast, the instruments being fixed on 1-m L-shaped brackets. The wind velocities were measured at least at 5 and up to 14 levels, using classical anemometers (A100R Vector Instrument®), the wind direction being measured at an intermediate level (W200P Vector Instrument®). Such instruments were previously successfully used for continuous measurements performed in arid areas, i.e., in severe conditions of wind velocity and sand or dust storms [*Rajot et al.*, 2003]. The consistency of measurements from all the anemometers was tested in natural conditions using a recently acquired and calibrated sensor as reference before the experiment. For more than 200 tested data averaged on 1min for each of the 13 anemometers, the correlation to the reference measurements was higher than 0.98 with a slope ranging from 0.97 to 1.01. Air temperatures were simultaneously measured at four levels using ventilated probes (ASPTC, Aspirated Shield with Fine Wire Thermocouple type chromel Constantan; Campbell®).

[50] The height of the highest anemometer and the number of anemometers were determined, for each site, as a function of the experimental conditions and mainly by the fetch for which the surface was found homogeneous and plane. The heights of the measurement levels were spaced in order to be as close as possible to a logarithmic scale, but practically the lowest levels were conditioned by the height of the instruments (>20 cm). For the vegetated surfaces, tests have been performed to evaluate whether the lowest wind measurement was relevant compared to the height of the vegetation and does not induce a bias in the aerodynamic roughness length retrieval.

[51] Since the aerodynamic roughness lengths were expected to be quite low for most of the sites, the determination of the heights of wind and temperature measurements must be as precise as possible. For the highest levels, the heights were measured by reference to the top of the mast while a precise (±1 mm) determination of the height relative to the ground level was performed with a theodolite for the

Table 5. Range of Wind Direction and Heights of the Air Temperature Probes and Anemometers for Each Site During the 2000 Experiment in South Tunisia

Site	Date of Measurements, mm/dd	Range of Wind Direction	Temperature Probe Height, m				Anemometer Height, m												
			T1	T2	T3	T4	V1	V2	V3	V4	V5	V6	V7	V8	V9	V10	V11	V12	V13	V14
S0	03/27 to 03/28	110°–200°	0.455	1.445	1.815	3.660	0.240	0.645	1.130	1.650	1.995	2.350	3.210	3.980	4.480	5.090	5.720	7.130	-	-
S01 high[a]	03/30 to 04/01	150° ± 10	-	-	1.879	4.070	-	-	-	-	-	-	2.450	3.110	3.750	4.390	5.200	6.070	7.190	9.020
S01 high[b]	03/30 to 04/01	360°±10	-	-	1.879	4.070	-	-	-	-	-	-	2.450	3.110	3.750	4.390	5.200	6.070	7.190	9.020
S2	04/01 to 04/03	80°–220°	0.728	1.093	1.770	4.040	0.390	0.580	0.915	1.281	1.630	1.958	2.299	2.954	3.489	4.347	5.127	5.977	7.187	9.017
S3	04/17 to 04/18	275°–360°	0.515	1.043	1.811	3.122	0.307	0.515	0.892	1.245	1.664	2.003	2.691	2.993	3.442	3.993	4.546	4.968	5.658	-
S4	04/06 to 04/08	60°–130°	0.553	0.991	1.731	3.970	0.682	0.950	1.207	1.606	1.942	2.390	2.959	3.440	4.290	5.105	6.206	7.490	-	-
S5	03/05 to 03/06	200°–360°	0.648	1.173	1.840	4.004	0.409	0.684	1.040	1.366	1.712	2.027	2.318	2.986	3.604	4.324	5.104	5.849	6.534	7.264
S7	04/14 to 04/15	275°–270°	0.506	1.078	2.004	3.884	0.304	0.525	0.893	1.273	1.653	2.184	2.736	3.576	4.204	5.092	6.042	6.936	-	-
S08 low[a]	04/15 to 04/17	80°–125°	0.545	1.175	1.853	4.178	0.199	0.398	0.736	1.125	1.579	2.050	-	-	-	-	-	-	-	-
S08 low[b]	04/15 to 04/17	120°–300°	0.545	1.175	1.853	4.178	0.199	0.398	0.736	1.125	1.579	2.050	-	-	-	-	-	-	-	-
S9	04/11 to 04/14	190°–197°	0.334	0.824	1.610	3.790	0.198	0.385	0.713	1.014	1.397	1.809	2.302	3.152	3.511	4.110	5.052	5.782	6.520	7.322
S10	04/08 to 04/09	100°–190°	0.517	1.046	1.775	4.615	0.403	0.588	0.906	1.237	1.589	1.956	3.115	3.740	4.259	4.935	5.633	6.639	7.697	

lowest levels (up to ~2 m). The ground level was determined as an average of nine theodolite measurements around the vertical position of the instruments. Additional measurements of the relative distance between the instruments have been performed.

[52] The number and level of the wind velocity and temperature measurements for the various sites are reported in Table 5. Lastly, data acquisition was performed with a data logger (CR10X Campbell®) allowing the registration of all the dynamic parameters averaged on 30 s with a 5-s scanning time.

2.2.2.3. Retrieval and Data Selection

[53] During the 2 or 3 days duration of the experiment on each site, the meteorological conditions were not constant, especially, wind direction and velocity changed. In addition, the stability conditions were also different throughout the day. Thus, the relevant data sets have been selected to obtain the best retrieval of aerodynamic roughness lengths based on the following different criteria.

[54] 1. The inversion of the dynamical parameters is performed only if the wind direction is facing the instruments within a range of variation of ±120° to exclude situations for which the experimental device could induce perturbation of the measurements.

[55] 2. Although the minimal wind velocity that anemometers can measure is 0.25 m s^{-1}, we considered a minimum wind velocity of 1 m s^{-1} is required to have a sufficient precision to obtain a correct wind profile. Thus the computation of Z_0 is performed only when all the anemometers have measured a wind velocity greater than 1 m s^{-1}.

[56] 3. The gradient method used for the inversion of the dynamical parameters assumes the use of at least 10-min wind velocity averages [*Wieringa*, 1993]. Thus we used 15-min averages for wind velocity and air temperature.

[57] 4. To increase the reliability of the results from the numerical retrieval, additional criteria on the retrieved parameters have been used. From a numerical point of view, the fitting of a 15-min data set has been considered as relevant only if (1) the average deviation between the measured and fitted wind velocities ($U_m(Z_i) - U_f(Z_i)$) is lower than 5% and if (2) the average deviation between the measured and fitted temperature gradients ($\Delta\theta_m(Z_i) - \Delta\theta_f(Z_i)$) is lower than 0.05°. Otherwise, the corresponding data set is rejected.

[58] 5. To discriminate the cases of free convection, the profiles for which the fitted wind friction velocity U^* is lower than 0.2 m s^{-1} were also rejected.

[59] Figure 6 provides an example of the reduction in data scattering when using such data selection procedures.

[60] Finally, the median and the associated standard deviation of the aerodynamic roughness lengths fitted for the selected data sets are computed and classified depending on the atmospheric stability conditions. Following *Karlsson* [1986], the stability conditions have been defined as a function of the range of the Richardson number and only the results obtained during unstable, near neutral and stable conditions were considered (i.e., $0.02 < R_i < 0.02$).

[61] Figure 7 provides comparisons between the measured and observed wind velocities and temperature gradients for near-neutral conditions. In near neutral condition, the wind velocity profile versus the logarithm of height is linear, and the theoretical profile fits very well the measure-

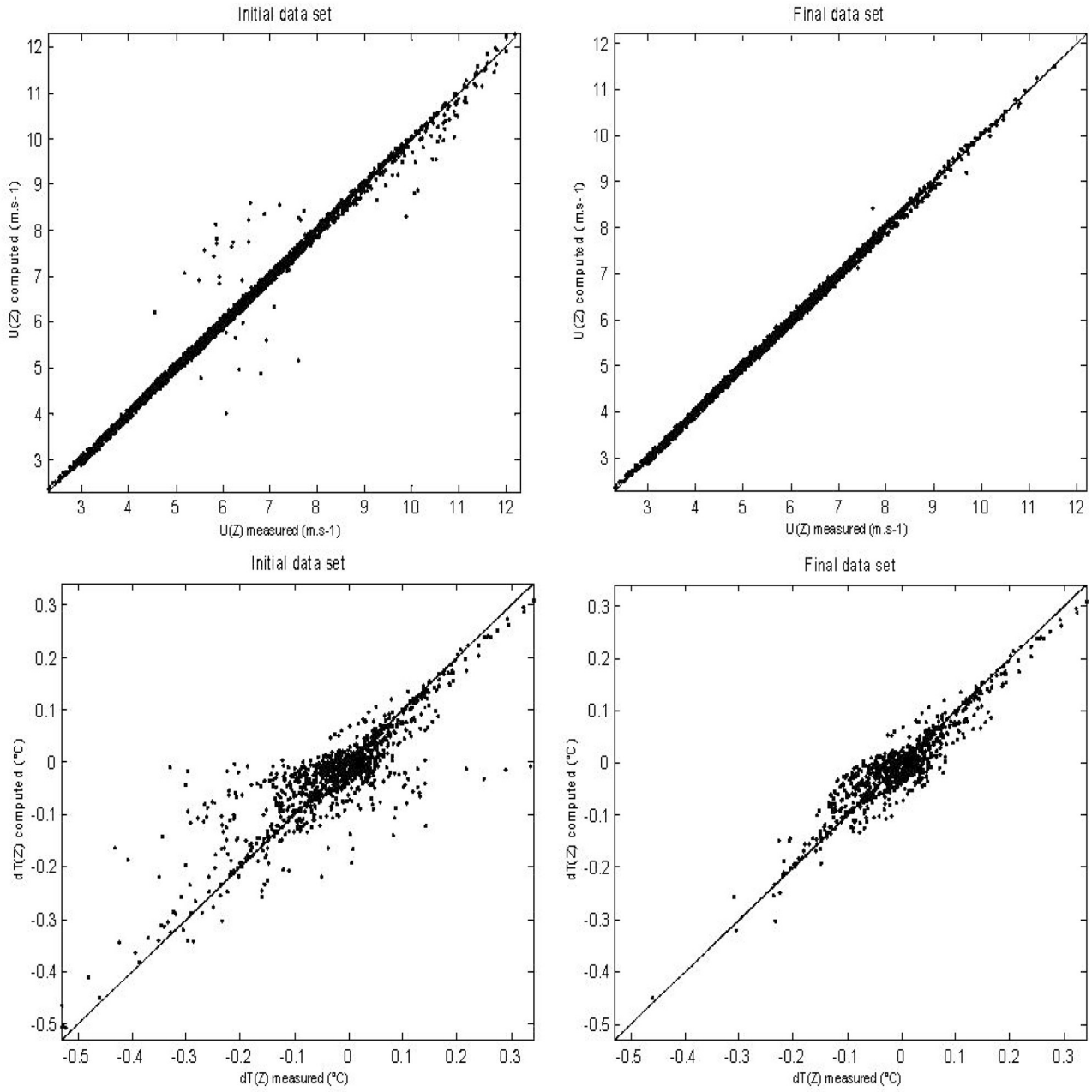

Figure 6. Measured versus fitted wind velocities and temperature gradients for site S10 before (initial data set) and after the data selection (final data set).

ments. The temperature gradients are very low, 0° to 0.02°C and the computed values match well the measurements.

[62] For the sites 1 (olive trees field) and 8 (dunes field), the surface is not isotropic, the geometry of the obstacles depending on the direction. Moreover, owing to the size of the olive trees and dunes, two different atmospheric layers were observed, one above and one below the obstacles. It was not possible to obtain a good fit of the wind profile for these two layers on the two sites. On the olive tree field, it was only possible to fit correctly the highest part of the wind profiles: According to the different wind directions, two different aerodynamic roughness lengths were retrieved, one corresponding to the closest tree direction (01 $high_a$), the other corresponding to the direction for which the next tree is along the diagonal tree (01 $high_b$). Similarly, two sectors have to be distinguished over the dunes field in the lowest boundary layer. They are referred as 08 low_a and 08 low_b, and correspond to different wind direction associated to differences in the height of the sand dunes.

2.2.2.4. Aerodynamic Roughness Length and Stability Conditions

[63] The aerodynamic roughness lengths retrieved over the various sites are reported in Table 6. A significant number of data inversions was performed for each site ($7 < n < 77$), except for site 9. For this site, the limited number of available data is due to an intense rain that

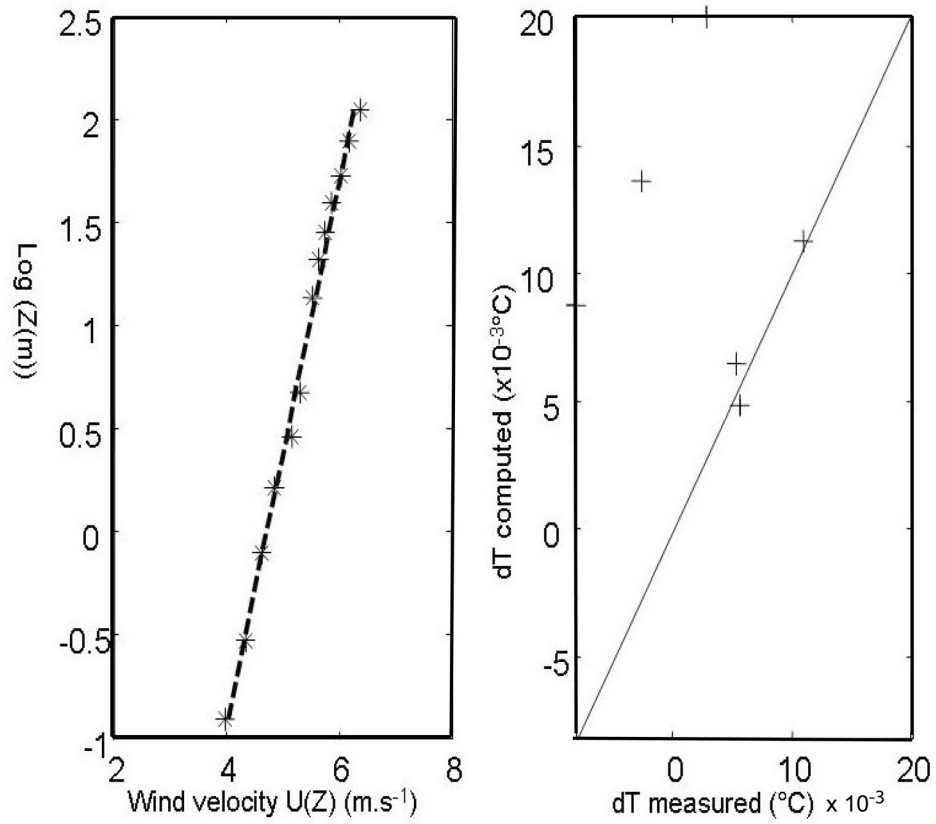

Figure 7. Wind velocities and temperature gradient vertical profiles for the site S10 for quasi neutral conditions. The dotted line in the left plot is the fitted profiles, and the solid line in the right plot is 1:1 slope. For this example, the retrieved dynamical parameters are $U^* = 0.31$ m s^{-1}, $T^* = 3.4 \times 10^{-3}$ °C, $Z_0 = 1.97 \times 10^{-3}$ m, and L = 1847 (wind direction = 136°).

occurred a few hours after the setup of the experiment. As a result, most of the measurements were performed over a moist surface, for which additional constraints on the soil and air relative humidity would have been necessary to precisely retrieve the aerodynamic roughness length.

[64] For all sites except site 3, a sufficient number of near-neutral situations occurred to accurately estimate the aerodynamic roughness length. For site 3, only stable or unstable conditions were encountered. The mean aerodynamic roughness lengths estimated for stable and unstable conditions for the other sites have been plotted as a function of the aerodynamic roughness length obtained in near neutral conditions (Figure 8). For most of the sites, the order of magnitude of the aerodynamic roughness length is correctly retrieved whatever the stability conditions except for sites 8 and 10 for which the underestimation can reach one or two orders of magnitude. It can be observed that stable conditions tend to provide slight underestimations of the aerodynamic roughness length (slope = 0.95) while unstable conditions induce slightly overestimated values

Table 6. Aerodynamic Roughness Lengths Retrieved for the Experimental Sites As a Function of the Stability Conditions[a]

	All Conditions			Near Neutral			Unstable			Stable		
Site	n	Mean, m	σ	n	Mean, m	σ	n	Mean, m	σ	n	Mean, m	σ
S0	15	6.34×10^{-3}	3.20×10^{-3}	12	6.73×10^{-3}	3.32×10^{-3}	-	-	-	3	5.36×10^{-3}	3.02×10^{-3}
S01 high[a]	6	3.56×10^{-2}	3.36×10^{-2}	3	3.91×10^{-2}	2.48×10^{-2}	-	-	-	3	2.27×10^{-2}	4.67×10^{-2}
S01 high[b]	10	3.53×10^{-1}	2.78×10^{-1}	3	5.95×10^{-1}	$1.20.10^{-2}$	3	4.72×10^{-1}	2.52×10^{-1}	-	-	-
S2	59	5.52×10^{-3}	3.50×10^{-3}	24	4.78×10^{-3}	2.62×10^{-3}	14	5.25×10^{-3}	1.34×10^{-3}	21	9.57×10^{-3}	3.81×10^{-3}
S3	7	4.60×10^{-3}	1.93×10^{-3}	-	-	-	2	4.69×10^{-3}	1.37×10^{-4}	5	3.85×10^{-3}	2.33×10^{-3}
S4	52	2.03×10^{-2}	4.89×10^{-3}	48	2.04×10^{-2}	3.63×10^{-3}	-	-	-	4	1.56×10^{-2}	1.41×10^{-2}
S5	41	1.45×10^{-2}	5.89×10^{-3}	19	1.67×10^{-2}	4.51×10^{-3}	6	1.07×10^{-2}	3.05×10^{-3}	16	1.08×10^{-2}	5.76×10^{-3}
S7	5	2.39×10^{-3}	2.39×10^{-3}	4	2.52×10^{-3}	2.10×10^{-4}	-	-	-	1	2.25×10^{-3}	-
S08 low[a]	26	1.24×10^{-5}	4.69×10^{-5}	8	1.88×10^{-5}	6.52×10^{-5}	3	6.41×10^{-5}	5.57×10^{-5}	15	7.43×10^{-6}	4.13×10^{-6}
S08 low[b]	77	1.56×10^{-4}	2.31×10^{-4}	40	3.42×10^{-4}	2.52×10^{-4}	14	1.84×10^{-4}	5.98×10^{-5}	23	7.02×10^{-6}	2.30×10^{-5}
S9	1	6.09×10^{-4}	-	1	6.09×10^{-4}	-	-	-	-	-	-	-
S10	51	1.65×10^{-3}	7.21×10^{-4}	46	1.73×10^{-3}	6.14×10^{-4}	-	-	-	5	2.38×10^{-4}	1.45×10^{-4}

[a]See text for details. For each site and stability criteria, the mean and standard deviation (σ) of the roughness length and the number of inverted data sets (n) are given. The indexes associated with the site number correspond to different wind direction range as described in Table 4.

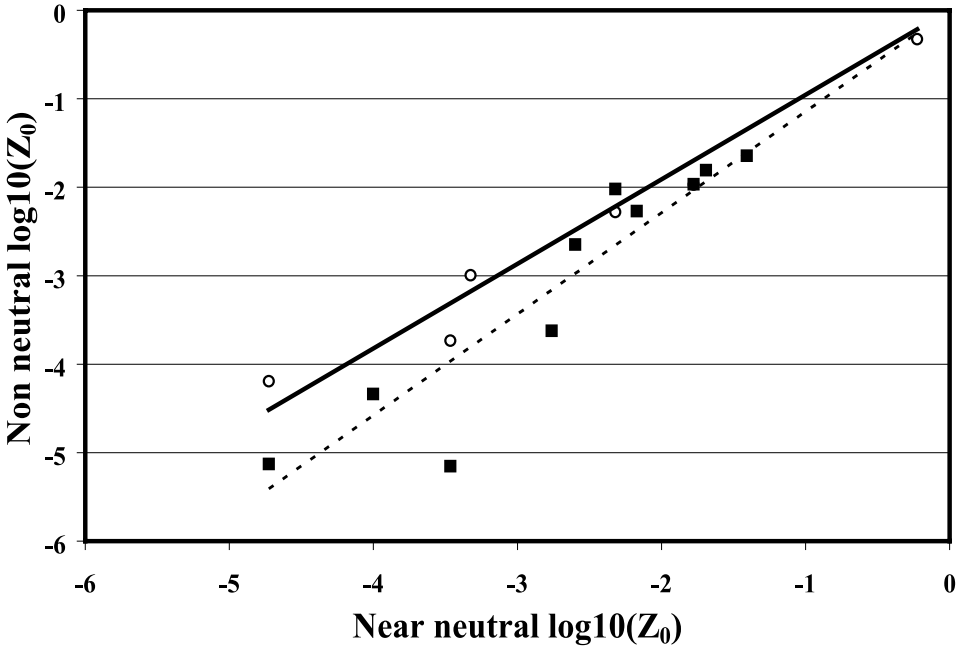

Figure 8. Comparison of the logarithm of the roughness height determined in near-neutral and in nonneutral conditions for sites S0, S1, S2, S4, S5, S7, S9, and S10 (white circle, unstable; black squares, stable; continuous line, linear fit for unstable conditions slope = 0.95, r = 0.98; dotted line, linear fit for stable conditions slope = 1.14, r = 0.93).

(slope = 1.14). We used these slopes as correction factors to estimate the "equivalent" near neutral values Z_0 of site 3. In stable conditions, the Z_0 is estimated to be 4.11×10^{-3} m while a value of 4.05×10^{-3} m is obtained for unstable conditions. These two values being very consistent, their average (4.08×10^{-3} m) will be considered as the best estimate of the aerodynamic roughness length for this site.

[65] For the whole data set, the uncertainties on the aerodynamic roughness lengths have been estimated from the standard deviation and the number of available data (Table 6) on the basis of the following equation:

$$\Delta Z_0 = \pm t^{\sigma_{Z_0}}/_{\sqrt{n}},$$

with t, the Student's t- test.

2.2.2.5. Comparison With Existing Data

[66] The aerodynamic roughness lengths retrieved for the different sites have been compared to published data. To make the comparison as relevant as possible, we selected the measurements of aerodynamic roughness length performed over natural surfaces with low vegetation cover or over unvegetated surfaces covered with gravel and cobbles (Table 7).

[67] For the dune field (site 8), our results (2×10^{-5} to 3×10^{-4} m) are in good agreement with those from the literature, in particular those obtained in Namibia (4×10^{-5} to 4×10^{-4} m) [*Greeley et al.*, 1997], China (3 to 4×10^{-4} m) [*Xian et al.*, 2002], Antarctica (5 to 9×10^{-4}) [*Lancaster*, 2004] and USA (7×10^{-4}) [*Lancaster and Baas*, 1998] for comparable sites (respectively, interdunal area, sandy surface with tiny cobbles, flat sand with scattered rocks, bare sand sheet). The values from the literature for salty depressions range from 1.3×10^{-4} m (Lunar Lake [*Greeley et al.*, 1997]) to 6.3×10^{-4} m (Confidence Mill Playa [*Greeley et al.*, 1988]). Our determination of the aerodynamic roughness length over the Chott El Jerid (site 9, 6×10^{-4} m) is of the same order of magnitude and agrees well with the higher limit of these measurements.

[68] The aerodynamic roughness lengths retrieved for vegetated and stony surfaces (sites 2, 3, 4, 5, 7 and 10) range from 1.7×10^{-3} m to 2×10^{-2} m. The values available in the literature for unvegetated surfaces with gravel and cobbles, are of the order of 5×10^{-4} to 3×10^{-2} m and they range from 10^{-3} to 2×10^{-2} for surfaces with low grass cover and from 2×10^{-3} to 7×10^{-2} m for surfaces with long grass or tundra. Our aerodynamic roughness length measurements are thus consistent with those published for gravel surfaces and surfaces with low vegetation cover.

3. Geometrical Roughness and Aerodynamical Roughness Length

[69] This field experiment provided coupled measurements of geometrical and aerodynamic roughness for six experimental sites. This experimental data set can used to test whether the empirical relationship established to link the roughness density to the aerodynamic roughness length and derived from wind tunnel measurements for artificial obstacles applies to natural surfaces.

3.1. Relation Between Aerodynamic Roughness Length and Geometric Dimensions of the Obstacles

[70] To estimate the aerodynamic roughness length for arid areas from the geometric dimensions of the roughness elements, *Marticorena et al.* [1997b] established an empir-

Table 7. Aerodynamic Roughness Heights and Associated Surface Types From the Literature for Sites With Surface Features Similar to the South Tunisian Sites

				This Work		
Reference	Site/Reference	Z_0, m	Surface Type	Site	Z_0 Min, m	Z_0 Max, m
Wieringa [1993]	*Tezlaff* [1974]	3.00×10^{-4}	flat desert	S8	1.88×10^{-5}	3.42×10^{-4}
	recommended by Wieringa	2×10^{-4} to 5×10^{-4}	very flat surfaces	S9	6.09×10^{-4}	6.09×10^{-4}
	Waranga [*Hicks*, 1976]	1.20×10^{-3}	flat surface with almost no grass	S2, S3, S4, S5, S7, S10	1.73×10^{-3}	2.04×10^{-2}
	recommended by Wieringa	1×10^{-3} to 4×10^{-3}	fallow ground	S0	6.73×10^{-3}	6.73×10^{-3}
	Deacon [1953]	2×10^{-3} to 1.7×10^{-2}	short grass	S2, S3, S4, S5, S7, S10	1.73×10^{-3}	2.04×10^{-2}
	Blackadar [1976]	1.00×10^{-2}	short grass	S2, S3, S4, S5, S7, S10	1.73×10^{-3}	2.04×10^{-2}
	Saugier and Ripley [1978]	1.10×10^{-2}	short grass	S2, S3, S4, S5, S7, S10	1.73×10^{-3}	2.04×10^{-2}
	Harper and Wiseman [1977, 1978]	2.10×10^{-2}	tundra	S2, S3, S4, S5, S7, S10	1.73×10^{-3}	2.04×10^{-2}
	recommended by Wieringa	8×10^{-3} to 3×10^{-2}	short grass; moss	S2, S3, S4, S5, S7, S10	1.73×10^{-3}	2.04×10^{-2}
	Pasquill [1950]	3×10^{-2} to 7×10^{-2}	long grass	S2, S3, S4, S5, S7, S10	1.73×10^{-3}	2.04×10^{-2}
Lancaster and Baas [1998]	Owens Lake	2×10^{-3} to 1.3×10^{-2}	sand sheet with salt grass	S2, S3, S4, S5, S7, S10	1.73×10^{-3}	2.04×10^{-2}
Greeley et al. [1988]	Amboy	1.73×10^{-3}	alluvial fan	S2, S3, S4, S5, S7, S10	1.73×10^{-3}	2.04×10^{-2}
	Lucerne	1.40×10^{-4}	Playa	S9	6.09×10^{-4}	6.09×10^{-4}
Greeley et al. [1991b]	Confidence Mill Playa	6.30×10^{-4}	playa	S9	6.09×10^{-4}	6.09×10^{-4}
	Confidence Mill Playa	1.80×10^{-4}	playa	S9	6.09×10^{-4}	6.09×10^{-4}
Greeley et al. [1997]	Stovepipe wells	2.46×10^{-3}	flat sand and gravel surface	S2, S3, S4, S5, S7, S10	1.73×10^{-3}	2.04×10^{-2}
	Kit Fox Fan	7.73×10^{-4}	gravel to cobble sandy surface	S2, S3, S4, S5, S7, S10	1.73×10^{-3}	2.04×10^{-2}
	Golden Canyon Fan	4.72×10^{-3}	alluvial fan with gravel to small boulders	S2, S3, S4, S5, S7, S10	1.73×10^{-3}	2.04×10^{-2}
	Lunar Lake	1.82×10^{-4}	playa	S9	6.09×10^{-4}	6.09×10^{-4}
	Lunar Lake	1.26×10^{-4}	playa	S9	6.09×10^{-4}	6.09×10^{-4}
	Gobabeb; Namibia	4.00×10^{-5}	interdunal surface	S8	1.88×10^{-5}	3.42×10^{-4}
	Gobabeb; Namibia	4.20×10^{-4}	desert flats	S8	1.88×10^{-5}	3.42×10^{-4}
Lancaster [2004]	McMurdo Dry Valley, Antartica	1×10^{-3} to 3×10^{-2}	gravelly sand sheets to boulder-covered moraines	S2, S3, S4, S5, S7, S10	1.73×10^{-3}	2.04×10^{-2}
	McMurdo Dry Valley, Antartica	5×10^{-4} to 9×10^{-4}	flat sand with scattered rocks	S8	1.88×10^{-5}	3.42×10^{-4}
Lancaster and Baas [1998]	Owens Lake	7.5×10^{-4}	bare sand sheet	S8	1.88×10^{-5}	3.42×10^{-4}
Xian et al. [2002]	Dunhuang Mogao Grottos, China	7×10^{-4} to 2×10^{-3}	gravel to cobble sandy surface	S2, S3, S4, S5, S7, S10	1.73×10^{-3}	2.04×10^{-2}
	Dunhuang Mogao Grottos, China	5×10^{-4} to 1×10^{-3}	flat sand and gravel surface	S2, S3, S4, S5, S7, S10	1.73×10^{-3}	2.04×10^{-2}
	Dunhuang Mogao Grottos, China	3×10^{-4} to 4×10^{-4}	sandy surface with tiny cobbles	S8	1.88×10^{-5}	3.42×10^{-4}

Table 8. Lateral Cover for Vegetation (L_{cv}) and for Pebbles and Gravel (L_{cb}), Total Lateral Cover ($L_{c\ tot}$), Mean Height for Vegetation (h_v) and for Pebbles (h_b), and Weighted Height and Ratio of the Pebble Lateral Cover L_{cb} to Total Lateral Cover $L_{c\ tot}$, Aerodynamic Roughness Height, and Ratio of the Roughness Height to the Weighted Height

Site	L_{cv}	h_v Mean, cm	L_{cp}	h_b Mean, cm	$L_{c\ tot}$	L_{cp}/tot	h Weight	Z_0, cm	Z_0/h Weight
S2	0.106	14.9	0.013	1.36	0.119	0.11	13.43	0.48	0.036
S3	0.056	11.0	0.041	0.88	0.097	0.42	6.70	0.41	0.069
S4	0.152	18.2	0.058	1.18	0.210	0.28	13.50	2.0	0.151
S5	0.071	15.4	0.162	1.99	0.233	0.70	6.08	1.7	0.275
S7	0.023	16.5	0.002	1.27	0.025	0.08	15.37	0.25	0.016
S10	0.037	9.4	0.031	1.17	0.068	0.46	5.62	0.17	0.031

ical relationship between L_c and the ratio of aerodynamic roughness length to the average height of the roughness elements Z_0/h_m. This relation was mainly derived from data obtained in wind-tunnel studies, using artificial roughness elements but also includes some data obtained over vegetated surfaces in semiarid areas [*Marshall*, 1971; *Jarvis et al.*, 1976; *Garratt*, 1977; *Raupach et al.*, 1980; *Raupach*, 1991; *Musick and Gillette*, 1990].

[71] As mentioned by *King et al.* [2005], an error was found in the computation of the aerodynamic roughness lengths performed by *Marticorena et al.* [1997b] for the data set by *Marshall* [1971]. This errors consists in a wrong reference height used in the retrieval of the roughness length from the wind friction velocity and the freestream wind velocity. This data set corresponds to the lowest lateral covers for which a linear relationship was obtained between Z_0/h_m and L_c. The data presented in this paper have thus been corrected and the numerical relationship initially obtained by *Marticorena et al.* [1997b] has been updated using almost the same data set than for the initial fitting as follows:

$$\text{For } L_c < 0.045 \qquad \log(Z_0/h_m) = 1.31\ \log(L_c) + 0.66 \quad (15)$$

$$\text{For } L_c \geq 0.045 \qquad \log(Z_0/h_m) = 1.16. \quad (16)$$

It must be noted that the recent experimental data set obtained for low values of L_c [*Minvielle et al.*, 2003] agrees well with these corrected estimations of the Marshall data set. The exhaustive wind tunnel data set summarized by *King et al.* [2005] also confirms the credibility of this relationship.

3.2. Results

[72] The main difficulty in comparing our data with this relationship is the determination of the mean height of the roughness elements. Indeed, the roughness elements present at the surface of our experimental sites exhibit very different sizes and are of different types (as, for example, vegetation and boulders). A reasonable assumption is to weight the height of the two types of roughness elements by their relative contribution to the lateral cover (Table 8). Making this assumption, we implicitly consider that the aerodynamic contributions of vegetation and boulders are identical when weighted by their respective L_c. This assumption is only valid if the porosity of the vegetation can be considered as negligible, i.e., lower than 20% [*Minvielle et al.*, 2003]. The results obtained for sites 4 and 5 tend to sustain this hypothesis. Both sites have comparable total L_c but vegetation contributes for less than 30% of the total L_c for site 4, and for more than 70% for site 5. Despite these differences in the fraction of L_c due to vegetation, comparable Z_0 have been retrieved over these two sites (2 cm for site 4 and 1.7 cm for site 5).

[73] For sites 2, 3, 4, 5, 7, 10 for which the experimental determination of the geometric roughness was performed, the aerodynamic roughness lengths have been plotted as a function of the total L_c (Figure 9a). Even if Z_0 correlates

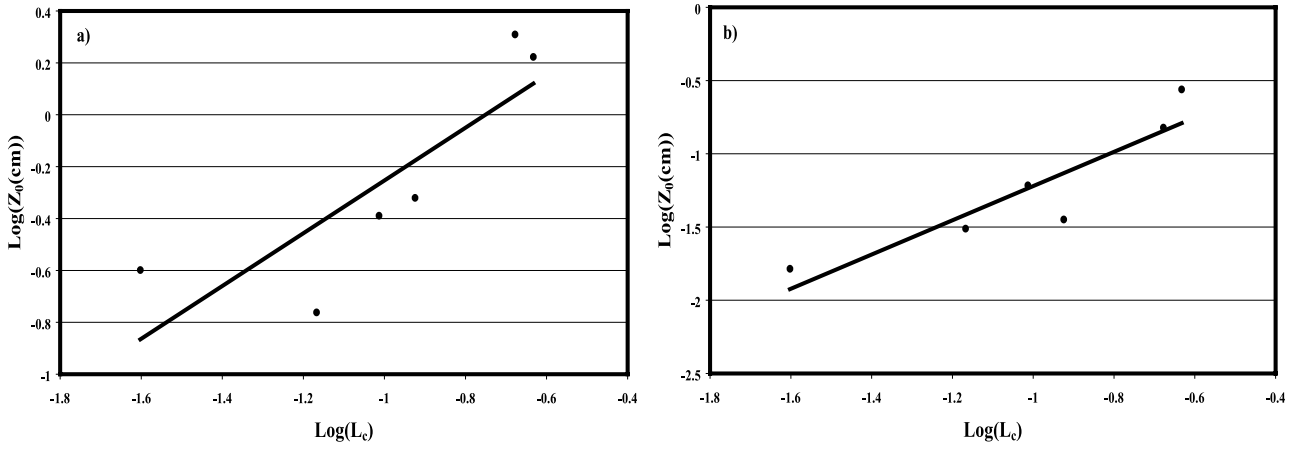

Figure 9. Logarithm (a) of the roughness height Z_0 and (b) of the ratio of roughness length to the mean height of the roughness elements as a function of the logarithm of the lateral cover.

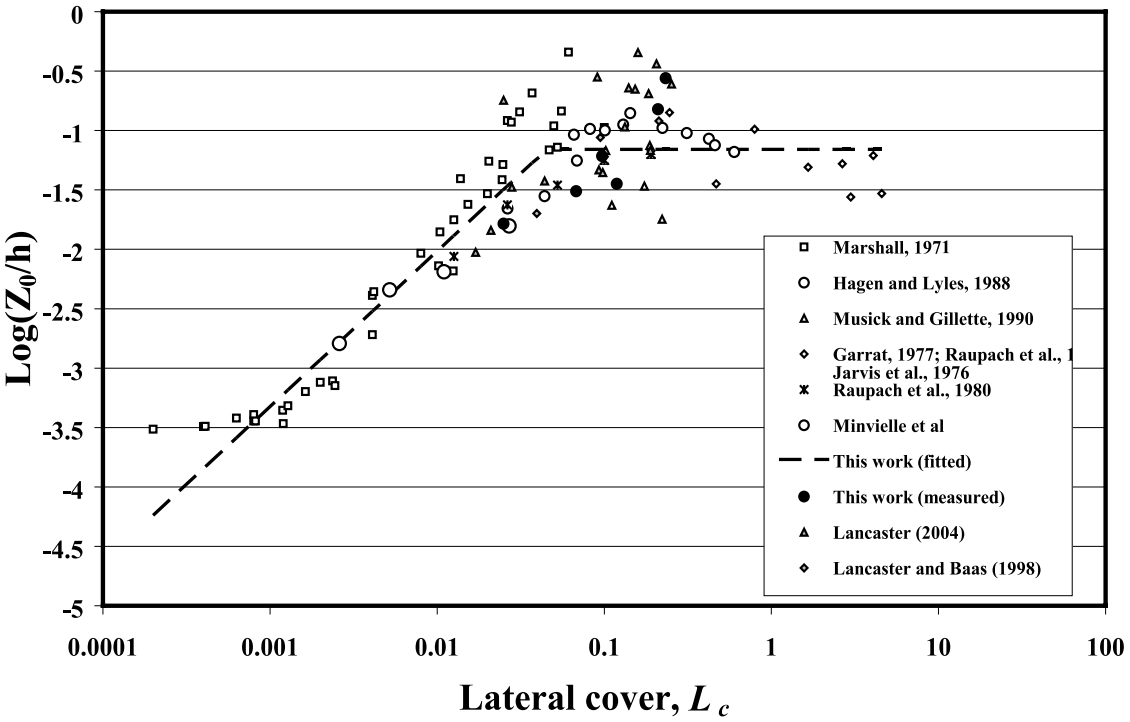

Figure 10. Logarithm of the ratio of the aerodynamic roughness height Z_0 to the mean roughness elements height as a function of the lateral cover (note that for the data corresponding to this work, the mean height is a weighted average for the two kinds of roughness elements (vegetation and pebbles)).

with L_c (r = 0.83), the data are less dispersed and the correlation is higher (r = 0.91) when the ratios Z_0/h_w are plotted as a function of L_c (Figure 9b).

[74] This clearly suggests that for a given roughness density, higher roughness elements will affect the aerodynamic roughness length more than smaller roughness elements having the same total frontal surface. This result is consistent with the analyses from *Musick et al.* [1996], who suggest the aspect ratio (height/width) of the vegetation elements as a key factor in the estimation of the reduction of the surface shear stress controlling the erosion thresholds.

[75] Our experimental results have been also compared to the previous experimental data used to fit equations (15) and (16) (Figure 10). They are also compared to field measurements obtained using similar methods over a vegetated surface [*Lancaster and Baas*, 1998] and over surfaces ranging from gravelly sand sheets to boulder covered moraines [*Lancaster*, 2004]. It is interesting to note that the experimental values obtained in natural conditions are quite consistent with the data derived from wind tunnel experiments using artificial compact roughness elements. This result indicates that the vegetation elements present on our experimental sites have an aerodynamic behavior similar to compact obstacles. This suggests that the effects of porosity and flexibility on their drag coefficient are limited, at least for this range of L_c. This also suggests that the fitted relationship can be used to estimate the aerodynamic roughness length over natural surfaces with a reasonable confidence level, provided that the geometric characteristics and the distribution of the roughness elements.

4. Relationship Between Surface Roughness and Radar Backscatter Coefficient

[76] The investigation of the relationship between the so-called aeolian roughness length and radar backscatter coefficient was initiated by *Greeley et al.* [1988]. The objective was to develop a technique for deriving aerodynamic roughness length for different geological surfaces from calibrated radar measurements. One application of such a technique was to map the aerodynamic roughness length and thus better predict the aeolian sand transport on Earth or on other planets. Indeed, other than radar sensor characteristics, radar backscattering over soil surface depends on surface properties such as dielectric constant, soil moisture and the surface roughness and on the local incident angle. In fact radar measured signal is not directly sensitive to aerodynamic roughness (which is not a parameter of surface but of wind). However, geometric roughness (that is the surface parameter) and aerodynamic roughness are linked, by erosion processes for instance.

[77] In the last years, various theoretical or empirical modeling approaches have been developed to investigate the relationships linking the effects of surface properties to the measured radar backscatter coefficients [*Fung et al.*, 1992; *Oh et al.*, 1992; *Zribi et al.*, 2000; *Zribi and Dechambre*, 2003]. For dry surfaces (like arid deserts) with low topography and comparable electromagnetic properties,

Table 9. Acquired SAR/ERS Images, and Local Incidence Angles at the Position of the Studied Sites[a]

Acquisition Date, yyyy/mm/dd	Orbit Number	Frame Number	Track	Number of Lines	Number of Columns	present Sites	Incidence Angles
1995/07/17	01250	2925	394	8221	7922	S9	-
1996/05/05	05444	2943	079	8220	7868	S0; S2; S5	21.6; 23.4; 21.9
1996/08/18	06947	2943	079	8222	7870	S0; S2; S5	21.7; 23.5; 21.9
1996/08/21	06990	2937	122	7785	7850	S7; S8	22.6; 23.7
1996/09/06	07219	2940	351	8222	7872	S10	22.2
1997/08/06	12000	2937	122	8191	7873	S7; S8	22.5; 23.7
1998/05/10	15965	2943	079	8224	7868	S0; S2; S5	21.7; 23.4; 21.9
1998/07/22	17010	2937	122	8202	7874	S7; S8	22.5; 23.7
1998/08/10	17282	2925	394	8226	7878	S9	-
1998/09/11	17740	2940	351	8218	7870	S10	22.2
1999/07/23	22249	2948	351	8222	7865	S3; S4	22.9; 21.1
2000/03/27	25799	2925	394	8218	7876	S9	-
2000/04/25	26214	2925	308	8223	7875	S1	-
2000/04/28	26257	2943	351	8219	7865	S3; S4; S10	22.9; 21.1; 22.1
2000/05/01	26300	2925	394	8213	7872	S9	-
2000/06/05	26801	2925	394	8212	7872	S9	-
2001/05/21	31811	2925	394	8133	7914	S9	-

[a]Sites do not include sites S0, S1 and S9, which have been given up in the following of the radar study.

the roughness effect dominates by far and the signal can be considered as a measure of the surface roughness at a scale comparable to the sensor wavelength [*Greeley et al.*, 1991].

[78] In the initial study performed by *Greeley et al.* [1988], backscatter coefficients were obtained from scatterometer data acquired in the L (λ = 19 cm), C (λ = 6.3 cm) and K (λ = 2.3 cm) bands by the NASA Johnson Space Centre Scatterometer over the Pisgah Lava field (California). This study supported the existence of a relationship between the aerodynamic roughness length and the radar backscatter coefficient at the L band direct polarization (HH) radar band frequencies. Additional radar data of the Pisgah lava field, the Amboy lava field and the Mojave deserts acquired in June 1998 by the NASA/JPL Airborne Synthetic Aperture Radar (AIRSAR) during the Mojave field experiment have been used by *Greeley et al.* [1991]. In order to investigate the sensitivity of the relationship to the microwave parameters, the authors used different calibrated multiple wavelength, polarization and incident angle radar data. The best relation was obtained for data acquired in L band, HV polarization and incidence angle around 35°. The Spaceborne Radar Laboratory (SLR) offered the opportunity to examine the consistency of these results for data obtained from orbit [*Greeley et al.*, 1997]. With SRL data, maximum correlation was found with L-HH and C-HV configurations. The authors derived a map of Z_0 for each experimental site, demonstrating the potential of radar systems onboard satellite to map Z_0 for large vegetation-free areas.

[79] Our objectives are (1) to further investigate the relationship between the aerodynamic roughness and radar backscatter coefficient based on the roughness field measurements obtained over partially vegetated surfaces and (2) to examine the capability of radar systems to retrieve the aerodynamic roughness length over arid and semi-arid areas when using an operational spaceborne instrument like the SAR/ERS sensor.

4.1. Radar Observations

[80] The SAR/ERS is a C-band sensor operating at 5.3 MHz (C band, wavelength equal to 5.66 cm). The size of an image is about 8000 by 8000 pixels and corresponds approximately to a 100 $\times$ 100 km^2 area, the size of each pixel being equal to 12.5 m $\times$ 12.5 m. Within the image the incidence angle ranges from 19° to 26°, being centered around 23°. Finally, the actual spatial resolution is equal to 30 m, and the radiometric resolution is around 1 dB. Table 9 reports the SAR/ERS database used for this study.

[81] The following data preprocessing steps have been performed.

[82] 1. Incidence angle corrections have been divided in two steps: a classical correction to account for the difference of geometrical surface contribution to the measured backscattering power [*Laur*, 1992] and a correction to account for the specific variation of σ_0 with incidence angle. This latter is performed using the theoretical Integral Equation Model (IEM [*Fung et al.*, 1992]). The model simulates the backscattering coefficient σ_0 as a function of the radar incidence angle α for different surface roughness, characterized by the standard deviation of surface height (or root mean square height), s and for different soil moistures. Figure 11 shows the variation of the simulated σ_0 as a function of α for s ranging from 0.2 cm to 1 cm with a 0.2-cm step. The soil moisture in the simulations is 0.05 cm^3 cm^{-3}, i.e., a typical value for a dry soil. For all the simulated cases, we observe a quasilinear relationship between the backscattering coefficient σ_0 and the radar incidence angle α with similar slopes. On the basis of this result, the variation of σ_0 with α has been approximated as linear, with a slope between 0.2 and 0.3.

[83] Local incidence angles at the location of the different sites in the different images have been estimated from orbit geometry (Table 9). As mentioned above, the sites have been selected to be as flat as possible to ensure the quality of the aerodynamic measurements, so no correction for the relief effect was necessary.

[84] The sites 1 (olive trees) and 9 (Chott Jerid) have not been considered in the following. Indeed, owing to the geometry of the olive tree field, it was not possible to derive a clear radar signal for site 1. For Chott Jerid, owing to nonnegligible and temporally variable soil moisture content, it was not possible to retrieve the contribution of the surface roughness to the radar backscatter coefficient with a good confidence level.

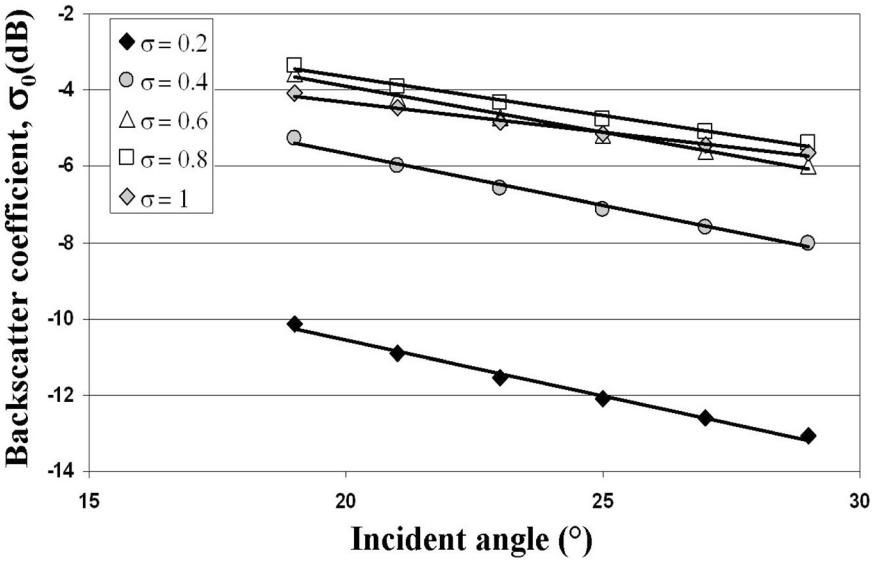

Figure 11. Variations of backscattering coefficient σ_0 (dB) versus incidence angle (degrees) as simulated with the theoretical Integral Equation Model (IEM [*Fung et al.*, 1992]).

[85] The different images corrected from the incidence angle effect are finally projected with the same geometry. When several images belong to the same track, they are superimposed by a simple translation. The translation vectors are found by maximizing the correlation. For the images belonging to different tracks, a second-order polynomial transformation is assumed, whose coefficients are found by minimizing a least squares error computed using reference points or targets. Finally, the precision of the image superposition ranges from 1 to 2 pixels both in line and column directions.

4.2. Relationship Between the Surface Roughness and the Radar Backscatter Coefficient

[86] The radar backscatter coefficients for the different images (i.e. different dates) are given for each site in Table 10. Each value corresponds to one radar measurement, σ_0, for a given site and a given orbit.

[87] For a given site, the temporal variations of the radar backscatter coefficient, as deduced from the values obtained for different dates, give an evaluation of the consistency of the signal. Especially, fluctuations of the soil moisture content with time could induce variations in the backscatter coefficient. We note that two sites (sites 10 and 0) exhibit a relatively high variability in the radar backscatter coefficient compared to the other sites. Concerning site 10, its location, close to relief areas, may lead to a weaker reliability of the location in the radar image (due to relief deformation), and subsequently a weak reliability of the estimated radar signal values. Moreover, it is an occasionally used pasture area for which the nomadic flocks may modify the soil roughness by crossing and overgrazing. Site 0 is located closed to the coast where precipitation is more frequent than on the other sites so the soil moisture is suspected to be responsible for these observed variations in the backscatter coefficients.

4.2.1. Relative Influence of the Geometric and Aerodynamic Roughness Length

[88] Figures 12 and 13 report the backscatter coefficients respectively as a function of the lateral cover and of the aerodynamic roughness length. Globally, the backscattered signal increases both with the geometric roughness (L_c) and the aerodynamic roughness (Z_0). This general trend of variation suggests that for the considered sites and selected periods, the soil moisture does not affect significantly the radar signal (very dry conditions leading to constant and negligible soil moisture). For both parameters, a log linear relationship was fitted on the available data, i.e., five sites for which L_c was estimated and eight sites for which Z_0 was

Table 10. Radar Backscatter Coefficients σ_0 for the Different Sites and the Different Orbits

Site	σ_0
S0	−13.20
S0	−12.45
S0	−13.43
S2	−12.76
S2	−13.37
S3	−8.63
S3	−8.27
S4	−8.50
S4	−8.20
S5	−8.79
S5	−8.94
S5	−8.66
S7	−15.60
S7	−16.16
S7	−16.07
S8	−17.94
S8	−17.66
S8	−17.78
S10	−12.03
S10	−14.24
S10	−13.68

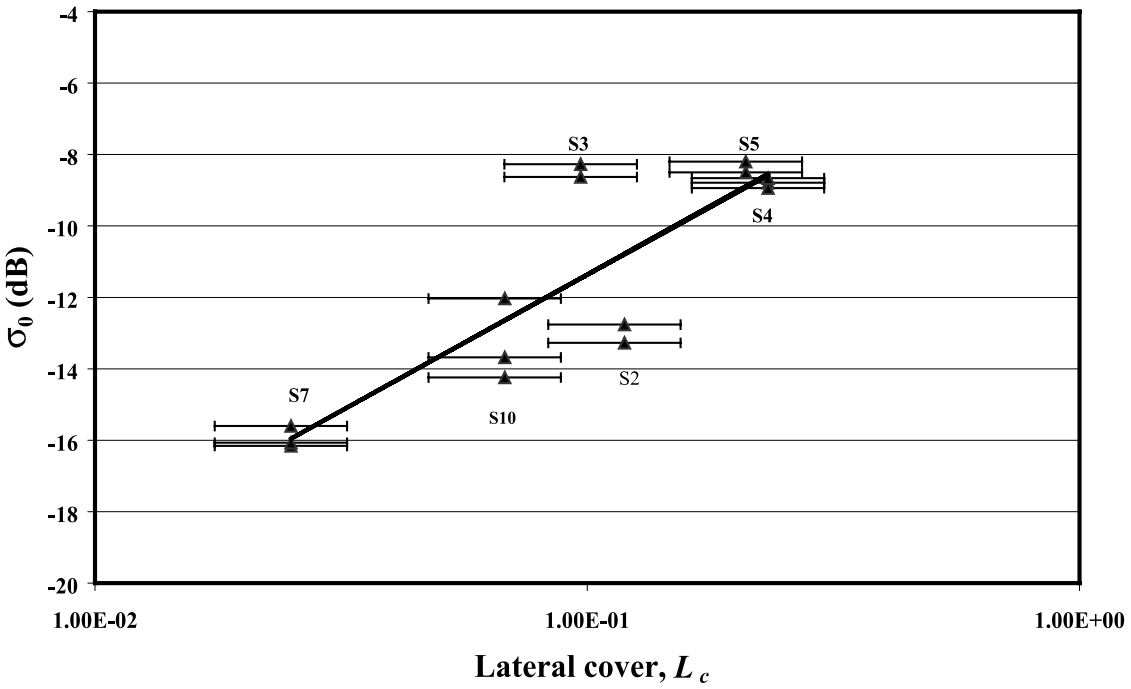

Figure 12. ERS/SAR backscattered signal σ_0 versus lateral cover, L_c from arid and semiarid sites of south Tunisia, (solid line: $\sigma_0 = 3.31 \ln(L_c) - 3.74$, r = 0.87, n = 14).

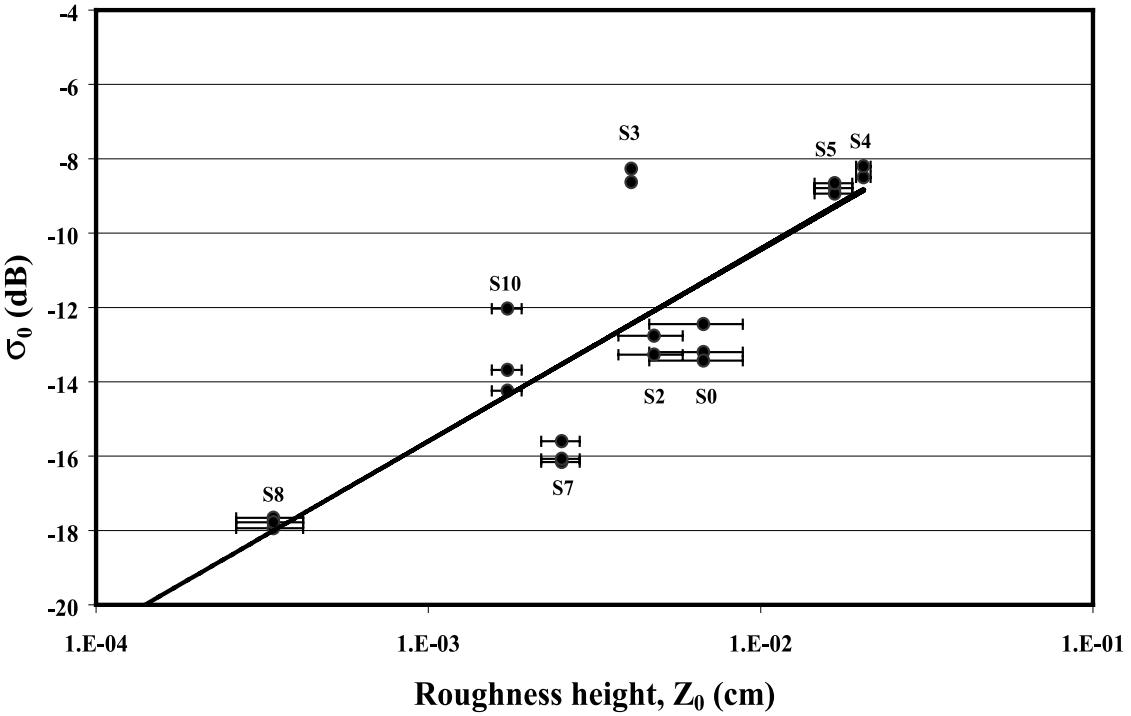

Figure 13. ERS/SAR backscattered signal σ_0 versus aerodynamic roughness height Z_0 (solid line: $\sigma_0 = 2.24 \ln(Z_0) - 0.11$, r = 0.84, n = 23).

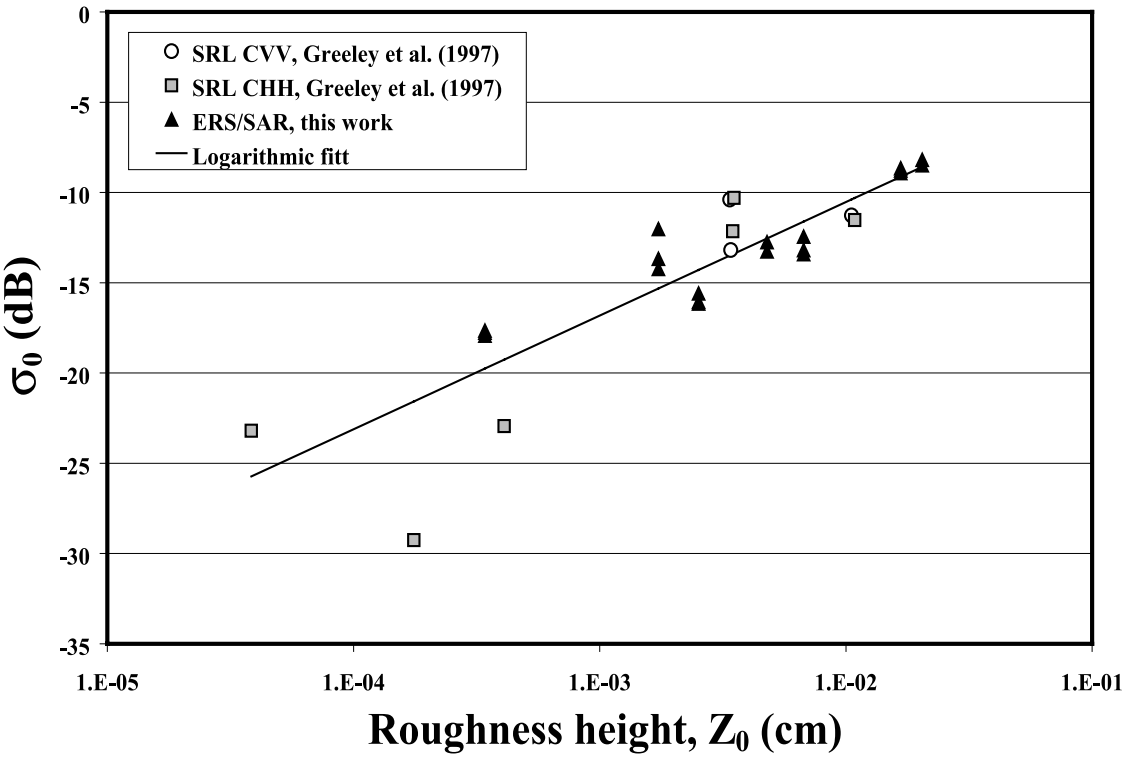

Figure 14. Radar backscattered signal σ_0 in dB versus aerodynamic roughness length Z0 (cm) for SRL data from *Greeley et al.* [1997] and from ERS/SAR (this work) (logarithmic fit: $\sigma_0 = 2.73 \ln(Z_0) + 2.05$, r = 0.88, n = 28).

derived from the wind profiles. The correlation coefficients of σ_0 with both L_c (r = 0.87, n = 14) and Z_0 (r = 0.84, n = 23) are highly significant suggesting that the retrieval of surface roughness over arid and semiarid areas from operational spaceborne radar instruments is valid. When the comparison is limited to the five sites for which both L_c and Z_0 are measured, comparable correlation coefficients are obtained. Thus it was not possible to separate from these results whether the radar signal is more sensitive to the geometrical or the aerodynamic roughness.

4.2.2. Empirical Relationship Between σ_0 and Z_0

[89] Two logarithmic relationships have been fitted on the experimental data points: a first one considering all available data (r = 0.84, n = 23), and a second one excluding site 3 for which the aerodynamic roughness length was only estimated during nonneutral conditions (r = 0.91, n = 21). In both cases, the fitted curve is logarithmic, and the slope is around 2.2 (respectively, 2.24 and 2.21). The least squares errors are, respectively, equal to 2.0 dB or 1.2 dB depending on the considered data set. These values should be compared to the ERS/SAR signal error bar (due to speckle, calibration errors, etc.) which generally ranges from 1 to 1.5 dB.

[90] *Blumberg and Greeley* [1993] obtained comparable relationships with airborne data from AIRSAR in the C band and VV polarization (slope = 2.27; r = 0.74, n = 16) and higher slope in HH polarization (slope = 2.76, r = 0.79, n = 15) and HV polarization (slope = 2.97, r = 0.8, n = 14). However, the individual data for the HH and VV polarization are very similar, since the mean ratio between the two values for the different aerodynamic roughness lengths is 1.03, while it is 1.8 when comparing the HV polarization data set to the HH or VV polarization data set. It must be noted that AIRSAR data have a more favorable incidence angle configuration (35°) than the ERS/SAR data we used (23°) since the signal sensitivity decrease with the incident angle. Another element in favor of AIRSAR is that the noise is lower on airborne sensors than for spaceborne sensors.

[91] *Greeley et al.* [1997] examined the relationship between the aerodynamic roughness lengths measured for four of the sites from *Blumberg and Greeley* [1993] and two sites in the Namibia Desert and the backscatter coefficients obtained with the SIR-C instrument onboard the Shuttle Radar Laboratory and the AIRSAR. As for the AIRSAR measurements, the mean ratio between the data in CHH (six points) and CVV polarization (three points) is 0.99, while the ratio between the data in CHV (six points) and CVV polarization (three points) is 1.77. These authors found a close correspondence between the SRL data and the relationship derived from AIRSAR data.

[92] Because both data sets involve spaceborne measurements, we compared our data to the SRL data set from *Greeley et al.* [1997] in CHH and CVV polarization (Figure 14). The two data sets exhibit the same variation of the backscatter coefficient as a function of the aerodynamic roughness length. The data are more dispersed in the range of low aerodynamic roughness lengths ($<10^{-3}$ cm). This can be explained by the difficulties of the aerodynamic roughness length retrieval over such surfaces and to the precision of the radar signal for such low values of σ_0.

[93] Finally, a high correlation is observed between the backscatter coefficient σ_0 and the aerodynamic roughness length Z_0, both for airborne and spaceborne measurements. When testing different wavelengths and polarization combinations in the AIRSAR data, *Greeley et al.* [1991] found that the best correlation was obtained in the L band. On the basis of these results and on additional SIR-C SRL measurements, *Greeley et al.* [1997] recommended the use of L-HV to map the aerodynamic roughness length at the local to regional scale. However, the authors noticed that relatively good correlations were obtained for other wavelength-polarization that could provide acceptable estimation of the aerodynamic roughness length. The relationship obtained in this work between SAR σ_0 and measured Z_0 is in close agreement with the one derived from *Greeley et al.* [1997] for σ_0 in the C band and HH and VV polarization. This shows that the C band radar measurements allow a reliable retrieval of the aerodynamic roughness length.

[94] When the two data sets are fitted together, the following relationship between σ_0 and Z_0 is obtained:

$$\sigma_0 = 2.73 \ln(Z_0) + 2.05, \quad (17)$$

with r = 0.88, n = 28. This relationship can be applied to backscatter coefficients from operational SAR sensors, such as the ERS/SAR for the mapping the aerodynamic roughness lengths for local to regional application. Such an approach could be extended to data from ENVISAT/ASAR which has a very close configuration (C band, several polarization and various incidence angles). It must be noted that our data set includes several sites with low permanent vegetation cover while the data sets from *Greeley et al.* [1991] and *Greeley et al.* [1997] only concerned bare surfaces. For sparse vegetation the measured signal depends on the vegetation features and on the soil backscattering signal attenuated by the vegetation layer. Fortunately, in the case of low incidence angles (like with ERS sensor), vegetation contribution could be neglected relative to the bare soil one [*Ulaby et al.*, 1986]. Thus our work suggests that equation (17) can be applied to retrieve the aerodynamic roughness lengths, not only for arid areas, but also for semiarid areas with low permanent vegetation cover (<25%).

5. Conclusion

[95] Field measurements of the lateral cover and aerodynamic surface roughness have been performed in arid and semiarid areas of southern Tunisia. Ten sites exhibiting a variety of surface features and roughness elements have been investigated for which both the geometric and the aerodynamic roughness have been experimentally determined.

[96] These measurements have been used to further investigate the relationship between the geometric and the aerodynamic roughness. Such a relationship between the ratio of aerodynamic roughness length to the mean height of the roughness elements and the lateral cover was previously suggested from wind tunnel data obtained mainly by using artificial obstacles [*Marticorena et al.*, 1997b]. The agreement between our experimental results and this relationship suggests that for the type of vegetation encountered in South Tunisia, other structural factors such as porosity or flexibility does not influence significantly the aerodynamic properties of the surface. In contrast, it suggests that the aspect ratio (height/width) of the roughness elements could significantly influence the surface roughness. Finally, it appears that the empirical relationship previously established allows reasonable estimations of the aerodynamic roughness length for natural surfaces based on the geometric characteristics of the roughness elements. This approach may constitute an valuable alternative to the wind profile measurements technique to estimate the aerodynamic roughness length for remote areas with severe climatic conditions such a dry hot deserts.

[97] This data set was also used to investigate the possible relationships linking the lateral cover and/or the aerodynamic roughness to radar backscatter coefficients. Satisfying relationships were found between the backscatter coefficients and both the lateral cover and the aerodynamic roughness length. Using different radar configurations with AIRSAR and SRL data, *Greeley et al.* [1995, 1997] and *Greeley and Blumberg* [1995] had established a log linear relationship between the aerodynamic roughness length and the radar backscatter coefficients. However, the feasibility of the retrieval of the aerodynamic roughness lengths from operational spaceborne radar instruments was not established. The aerodynamic roughness lengths measured in Tunisia and the radar backscatter coefficients obtained by the SAR/ERS sensor at 5.3 MHz in the C band are highly correlated confirming the sensitivity of spaceborne radars to surface roughness in arid and semi-arid areas. The SAR/ERS data set has been found in close agreement with the SIR-C SLR data set from *Greeley et al.* [1997]. On the basis of these two data sets which include data corresponding to different arid and semiarid areas (North Africa, South Africa, North America), we propose an empirical relationship to retrieve the aerodynamic roughness lengths using radar observations in the C band, from operational sensors such as ERS/SAR, ENVISAT/ASAR or RadarSAT. Note that the derived relationship has been proposed and validated for the ERS configuration (23° incidence angles, VV polarization, C band). The use of another sensor with different wave features would require a calibration of the relationship between the radar signal and the aerodynamic roughness length. The work of surface characterization and wind profile measurements done in this study can be used for such a calibration. The "operational" relationship proposed in this work can be used for the mapping of the aerodynamic roughness lengths for local to regional applications with a high spatial resolution. This approach will certainly provide a better assessment of the wind threshold friction velocities for aeolian erosion over arid and semiarid areas and thus significantly improve the modeling of the mineral dust cycle.

[98] **Acknowledgments.** This work was supported by the Programme National de Télédétection Spatiale of the French Centre National de la Recherche Scientifique and by the French Ministère de l'Education Nationale, de la Recherche et de la Technologie in the framework of a specific action "Coup de Pouce à la Recherche." The cooperation with the Institut des Régions Arides (Médénine, Tunisia) was supported by the Direction des Relations Européennes et Internationales of the French Centre National de la Recherche Scientifique in the framework of a "Programme Internationale de Coopération."

References

Arya, S. P. (1988), *Introduction to Micrometeorology*, 307 pp., Elsevier, New York.

Blackadar, A. K. (1976), Modeling the nocturnal boundary layer, paper presented at Third Symposium on Atmospheric Turbulence and Air Quality, Am. Meteorol. Soc., Boston, Mass.

Blumberg, D. G., and R. Greeley (1993), Field studies of aerodynamic roughness length, *J. Arid Environ.*, *25*, 39–48.

Callot, Y., B. Marticorena, and G. Bergametti (2000), Geomorphologic approach for modelling the surface features of arid environments in a model of dust emissions: Application to the Sahara desert, *Geodin. Acta*, *13*, 245–270.

Deacon, E. L. (1953), Vertical profiles of the mean wind in the surface layers of the atmosphere, *Geophys., Mem. 91*, Meteorol. Off., H.M Stationery Off., U. K.

Escadafal, R. (1989), *Caractérisation de la Surface des Sols Arides par Observations de Terrain et Télédétection*, 317 pp., Inst. Fr. de Rech. Sci. pour le Dev. en Coop. (ORSTOM), Bondy, France.

Frangi, J. P., and D. C. Richard (2000), The WELSONS experiment: Overview and presentation of first results on the surface atmospheric boundary-layer in semiarid Spain, *Ann. Geophys.*, *18*, 365–384.

Fung, A. K., Z. Li, and K. S. Chen (1992), Backscattering from a randomly rough dielectric surface, *IEEE Trans. Geosci. Remote Sens.*, *30*, 356–369.

Garratt, J. R. (1977), Aerodynamic roughness and mean monthly surface stress over Australia, *Tech. Pap 29*, Div. of Atmos. Phys., Commonw. Sci. and Ind. Res. Org., Melbourne, Australia.

Gillies, J. A., N. Lancaster W. G. Nickling, and D. M. Crawley (2000), Field determination of drag forces and shear stress partitioning effects for a desert shrub (*Sarcobatus vermiculatus*, Greasewood), *J. Geophys. Res.*, *105*, 24,871–24,880.

Greeley, R., and D. G. Blumberg (1995), Preliminary analysis of Shuttle Radar Laboratory (SRL-1) data to study aeolian features and processes, *IEEE Trans. Geosci. Remote Sens.*, *33*, 927–933.

Greeley, R., N. Lancaster, R. J. Sullivan, R. S. Saunders, E. Theilig, S. Wall, A. Dobrovolski, B. R. White, and J. D. Iversen (1988), A relationship between radar backscatter and aerodynamic roughness: Preliminary results, *Geophys. Res. Lett.*, *15*, 565–568.

Greeley, R., et al. (1991), Assessment of aerodynamic roughness via airborne radar observations, *Acta Mech.*, *2*, suppl., 77–88.

Greeley, R., D. G. Blumberg, A. R. Dobrovolski, L. R. Gaddis, J. D. Iversen, N. Lancaster, K. R. Rasmussen, R. S. Saunders, S. D. Wall, and B. R. White (1995), Potential transport of windblown sand: influence of surface roughness and assessment with radar data, in *Desert Aeolian Processes*, edited by P. Vatche Tchakerian, pp. 75–99, CRC Press, Boca Raton, Fla.

Greeley, R., D. G. Blumberg, J. F. McHone, A. Dobrovolski, J. Iversen, N. Lancaster, K. R. Rasmussen, S. Wall, and B. White (1997), Applications of spaceborne radar laboratory data to the study of aeolian processes, *J. Geophys. Res.*, *102*, 10,971–10,983.

Gueddari, M. (1984), Géochimie et thermodynamique des évaporites continentales: Etude du lac Natron (Tanzanie) et du Chott el Jerid (Tunisie), Ph.D. thesis, 152 pp., Univ. Louis Pasteur, Strasbourg, France.

Hagen, L. J., and L. Lyles (1988), Estimating small grain equivalents of shrub dominated rangeland for wind erosion control, *Trans. ASAE*, *31*, 769–775.

Harper, J. R., and W. J. Wiseman (1977), Temporal variation of surface roughness over a tundra surface, *J. Geophys. Res.*, *82*, 3495–3497.

Harper, J. R., and W. J. Wiseman (1978), Correction to "Temporal variation of surface roughness over a tundra surface", *J. Geophys. Res.*, *83*, 968.

Hicks, B. B. (1976), Wind profile relations from the Wangara experiment, *Q. J. R. Meteorol. Soc.*, *102*, 535–551.

Jarvis, P. G., G. B. James, and J. J. Landsberg (1976), Coniferous forest, in *Vegetation and the Atmosphere*, vol. 2, pp. 171–240, edited by J. L. Monteith, Elsevier, New York.

Karlsson, S. (1986), The applicability of wind profile formulas to an urban-rural interface site, *Boundary Layer Meteorol.*, *34*, 333–355.

King, J., W. G. Nickling, and J. A. Gillies (2005), Representation of vegetation and other nonerodible elements in aeolian shear stress partitioning models for predicting transport threshold, *J. Geophys. Res.*, *110*, F04015, doi:10.1029/2004JF000281.

Lancaster, N. (2004), Relation between aerodynamic and surface roughness in hyper-arid cold desert: McMurdo dry valleys, Antarctica, *Earth Surf. Processes Landforms*, *29*, 853–867.

Lancaster, N., and A. Baas (1998), Influence of vegetation cover on sand transport by wind: Field studies at Owens Lake, California, *Earth Surf. Processes Landforms*, *23*, 69–82.

Laur, H. (1992), ERS-1 SAR Calibration: Derivation of backscattering coefficient sigma-nought in ERS-1.SAR.PRI products, *ESA/ESRIN Tech. Note 1*, rev. 0, Eur. Space Agency, Paris.

Marshall, J. K. (1971), Drag measurements in roughness arrays of varying density and distribution, *Agric. Meteorol.*, *8*, 269–292.

Marticorena, B., and G. Bergametti (1995), Modeling the atmospheric dust cycle: 1. Design of a soil derived dust production scheme, *J. Geophys. Res.*, *100*, 16,415–16,430.

Marticorena, B., G. Bergametti, D. A. Gillette, and J. Belnap (1997a), Factors controlling threshold friction velocities in semi-arid areas of the United States, *J. Geophys. Res.*, *102*, 23,277–23,288.

Marticorena, B., G. Bergametti, B. Aumont, Y. Callot, C. N'Doumé, and M. Legrand (1997b), Modeling the atmospheric dust cycle: 2. Simulation of Saharan sources, *J. Geophys. Res.*, *102*, 4387–4404.

Millington, A. C., N. A. Drake, J. R. G. Townshend, N. A. Quarmby, J. J. Settl, and A. J. Reading (1989), Monitoring salt playa dynamics using Thematic Mapper data, *IEEE Trans. Geosci. Remote Sens.*, *27*, 754–761.

Minvielle, F., B. Marticorena, D. A. Gillette, R. Lawson, R. Thompson, and G. Bergametti (2003), Relationship between the aerodynamic roughness length and the roughness density in cases of low roughness density, *Environ. Fluid Mech.*, *3*, 249–267.

Monin, S. A., and A. M. Obukhov (1954), Basic turbulent mixing laws in the atmospheric surface layer, *Trans. Geofiz. Inst. Akad. Nauk.*, *24*(151), 163–187.

Musick, H. B., and D. A. Gillette (1990), Field evaluation of relationships between a vegetation structural parameter and sheltering against wind erosion, *Land Degrad. Rehabil.*, *2*, 87–94.

Oh, Y., K. Sarabandi, and F. T. Ulaby (1992), An empirical model and an inversion technique for radar scattering from bare soil surfaces, *IEEE Trans. Geosci. Remote Sens.*, *30*, 370–381.

Panofsky, H. A., and J. A. Dutton (1984), *Atmospheric Turbulence: Models and Methods for Engineering Applications*, 397 pp., John Wiley, Hoboken, N. J.

Pasquill, F. (1950), The aerodynamic drag of grassland, *Proc. R. Soc., Ser. A*, *202*, 143–153.

Rabia, M. C., and F. Zargouni (1990), Cartographie du couvert sédimentaire dans le Chott Jerid et ses environs (Sud Tunisien) par télédétection, in *Apports de la télédétection à la lutte contre la sécheresse*, *Actes des Journées scientifiques du réseau "Télédétection" de l'AUF*, pp. 253–263, John Libbey Eurotext, Paris.

Rajot, J. L., S. C. Alfaro, L. Gomes, and A. Gaudichet (2003), Soil crusting on sandy soils and its influence on wind erosion, *Catena*, *53*, 1–16.

Raupach, M. R. (1991), Saltation layers, vegetation canopies and roughness lengths, *Acta Mech.*, *1*, suppl., 83–96.

Raupach, M. R. (1992), Drag and drag partition on rough surfaces, *Boundary Layer Meteorol.*, *60*, 375–395.

Raupach, M. R., A. S. Thom, and I. Edwards (1980), A wind-tunnel study of turbulent flow close to regularly arrayed rough surfaces, *Boundary Layer Meteorol.*, *18*, 373–397.

Raupach, M. R., D. A. Gillette, and J. F. Leys (1993), The effect of roughness elements on wind erosion threshold, *J. Geophys. Res.*, *98*, 3023–3029.

Saugier, B., and E. A. Ripley (1978), Evaluation of the aerodynamic method of determining fluxes over natural grassland, *Q. J. R. Meteorol. Soc.*, *104*, 257–270.

Shao, Y. (2001), A model for mineral dust emission, *J. Geophys. Res.*, *106*, 20,239–20,254.

Shao, Y., M. R. Raupach, and J. F. Leys (1996), A model for predicting aeolian sand drift and dust entrainment on scales from paddock to region, *Aust. J. Soil Res.*, *34*, 309–342.

Tezlaff, G. (1974), Der wärmehaushalt in der zentralen Sahara, *Ber. Inst. Meteorol. Klimatol. Univ. Hanover*, *13*, 113 pp.

Ulaby, F. T., R. K. Moore, and A. K. Fung (1986), *Microwave Remote Sensing: Active and Passive*, Artech House, Norwood, Mass.

Wieringa, J. (1993), Representative roughness parameters for homogeneous terrains, *Boundary Layer Meteorol.*, *63*, 323–363.

Wolfe, S. A., and W. G. Nickling (1996), Shear stress portioning in sparsely vegetated desert canopies, *Earth Surf. Processes Landforms*, *21*, 607–619.

Xian, X., W. Tao, S. Qingwei, and Z. Weimin (2002), Field and wind-tunnel studies of aerodynamic roughness length, *Boundary Layer Meteorol.*, *104*, 151–163.

Zribi, M., and M. Dechambre (2003), A new empirical model to retrieve soil moisture and roughness from radar data, *Remote Sens. Environ.*, *84*, 42–52.

Zribi, M., V. Ciarletti, and O. Taconet (2000), Validation of a rough surface model based on fractional Brownian geometry with SIRC and ERASME radar data over Orgeval site, *Remote Sens. Environ.*, *73*, 65–72.

G. Bergametti, B. Marticorena, and M. Maillé, Laboratoire Interuniversitaire des Systèmes Atmosphériques, Universités Paris VII-XII, UMR CNRS 7583, 61 Avenue du General de Gaulle, F-94010 Créteil, France.

(bergametti@lisa.univ-paris12.fr; marticorena@lisa.univ-paris12.fr; maille@lisa.univ-paris12.fr)

Y. Callot, Université Lyon 2, Faculté GHHAT et Laboratoire IRG, F-69679 Bron, France. (Yann.Callot@univ-lyon2.fr)

P. Chazette, Laboratoire des Sciences du Climat et de l'Environnement, Commissariat à l'Energie Atomique, UMR CNRS 1572, Saclay, France.

M. Kardous and H. Khatteli, Institut des Régions Arides, 4119 Médénine, Tunisia. (mouldi.kardous@ira.rnrt.tn; Houcine.khatteli@ira.rnrt.tn)

S. Le Hégarat-Mascle and M. Zribi, Centre d'étude des Environnements Terrestre et Planétaires, UMR CNRS 8639, F-78140 Vélizy, France. (sylvie.mascle-lehegarat@cetp.ipsl.fr; mehrez.zribi@cetp.ipsl.fr)

J.-L. Rajot, Institut pour la Recherche et le Développement, Avenue de Maradi, BP 11416 Niamey, Niger. (rajot@ird.ne)

D. Vidal-Madjar, Direction des Ressources Humaines, CNRS, 3 Rue Michel-Ange, F-75016 Paris, France. (daniel.vidal-madjar@cnrs-dir.fr)